Author/s:
Zhang, H;Kinnear, C;Mulvaney, P

Title:
Fabrication of Single-Nanocrystal Arrays

Date:
2020-05-01

Citation:
Zhang, H., Kinnear, C. & Mulvaney, P. (2020). Fabrication of Single-Nanocrystal Arrays. Advanced Materials, 32 (18), https://doi.org/10.1002/adma.201904551.

Persistent Link:
https://hdl.handle.net/11343/286456

DOI: 10.1002/adma.201904551

Article type: Review

Fabrication of Single Nanocrystal Arrays

Heyou Zhang[1], Calum Kinnear[2] and Paul Mulvaney[1]

[1] ARC Centre of Excellence in Exciton Science, School of Chemistry, University of Melbourne, Parkville, VIC, 3010, Australia.

[2] CSIRO Manufacturing, Ian Wark Laboratories, Bayview Avenue, Clayton, Victoria 3168, Australia

mulvaney@unimelb.edu.au

Keywords

nanofabrication, direct assembly, arbitrary nano unit fabrication, nanocrystals, arrays, electrophoresis

Abstract

To realise the full potential of nanocrystals in nanotechnology, it is necessary to integrate single nanocrystals into addressable structures, for example arrays and periodic lattices. Here, the current methods for achieving this are reviewed. It is shown that a combination of top-down lithography techniques with directed assembly offers a platform for attaining this goal. The most promising of these directed assembly methods are reviewed: capillary force assembly, electrostatic assembly, optical printing, DNA-based assembly, and electrophoretic deposition. The last of these appears to offer a generic approach to fabrication of single nanocrystal arrays.

1. Introduction

Over the last two decades, nanocrystal science has blossomed into one of the most important fields in materials science due to the remarkable size effects such materials can exhibit. For example, metallic nanocrystals have unique plasmonic,[1] catalytic,[2] electronic and optical[3] properties, while semiconductor nanocrystals exhibit quantum confinement effects with potential applications in display technologies[4] and solar energy conversion.[5] However, it has become increasingly evident that a major bottleneck in the application of nanocrystals is their assembly. While it is straightforward to fabricate films or composites from nanocrystals, it is much more difficult to position single nanocrystals on a surface. This is a pre-requisite for applications in single molecule detection, high-density data storage, as single photon sources, and in quantum computation. A new form of nanofabrication is required that can facilitate and enable single nanocrystal positioning.

Nanofabrication tools,[6] born from rapid developments in microelectronics from the 1960s through to the 1990s, are now routinely accessible at institutions across the world. The specific technology that relates to pattern replication at the nanoscale is termed lithography and encompasses electron-beam lithography, photolithography, and nanosphere lithography, amongst others.[7] We can broadly classify nanofabrication methods into two categories. The first is self-assembled, template-based nanofabrication, where a self-assembled superstructure templates the deposition of a nanomaterial. Examples of this include nanosphere lithography for hexagonal structure fabrication,[8] sol-gel structures for creating porous templates,[9] fast pyrolysis for creating hollow structures,[10] and DNA-scaffolding.[11] These template-based processes are widely used due to their simplicity, low fabrication cost, and readily controlled pattern size. However, such methods can often only be used to template a limited range of patterns and offer little control over the final nanomaterial morphology.[6a] The second category we call "arbitrary unit nanofabrication". This refers to any process that is based on a hard template, which is patterned "arbitrarily" using electron beam lithography (EBL) or focused ion beam lithography (FIB). Due to the independent and deterministic fabrication of each unit, arbitrary unit nanofabrication enables the construction of more sophisticated nanostructures than soft-templated processes – in terms of dimensions, morphology, materials, and higher-order structures. Many studies have demonstrated the power of such arbitrary unit-based nanofabrication for applications such as plasmonic coupling,[12] optical and display devices,[13] and sensors.[14]

Both of the above nanofabrication strategies (soft template fabrication and lithograph-based fabrication) typically produce templates through which material is deposited via top-down evaporative processes, e.g. physical vapor deposition (PVD). However, such deposition processes offer only a limited range of possible material combinations and there is no control over crystallinity and only poor control over the nanocrystal morphology. The converse is true for nanocrystals synthesized in solution where there is a high degree of control over nanocrystal size, morphology, and crystallinity. Furthermore, complex materials such as core-shell nanocrystals are impossible to make via PVD processes but are easily synthesized chemically. Therefore, combining top-down lithography nanofabrication tools with "bottom-

up synthesized" nanocrystals appears to combine the best of both approaches, offering near-endless possibilities for nanofabrication and providing a robust platform for breaking the current bottlenecks in nanomaterials assembly. However, unifying both approaches introduces a range of challenges.

In this review, we summarize recent progress in the directed assembly of single nanocrystals. We begin by presenting some recent developments in standard, top-down nanofabrication methods, then we introduce various directed assembly methods for creating single nanocrystal arrays: capillary force assembly, electrostatic assembly, optical printing, DNA-based assembly, and electrophoretic deposition. Of these, the last one has the potential to become a robust, universal method for assembling single nanocrystals directly from solution.

2. The Role of Fabrication in Nanotechnology

2.1 The development of arbitrary unit nanofabrication

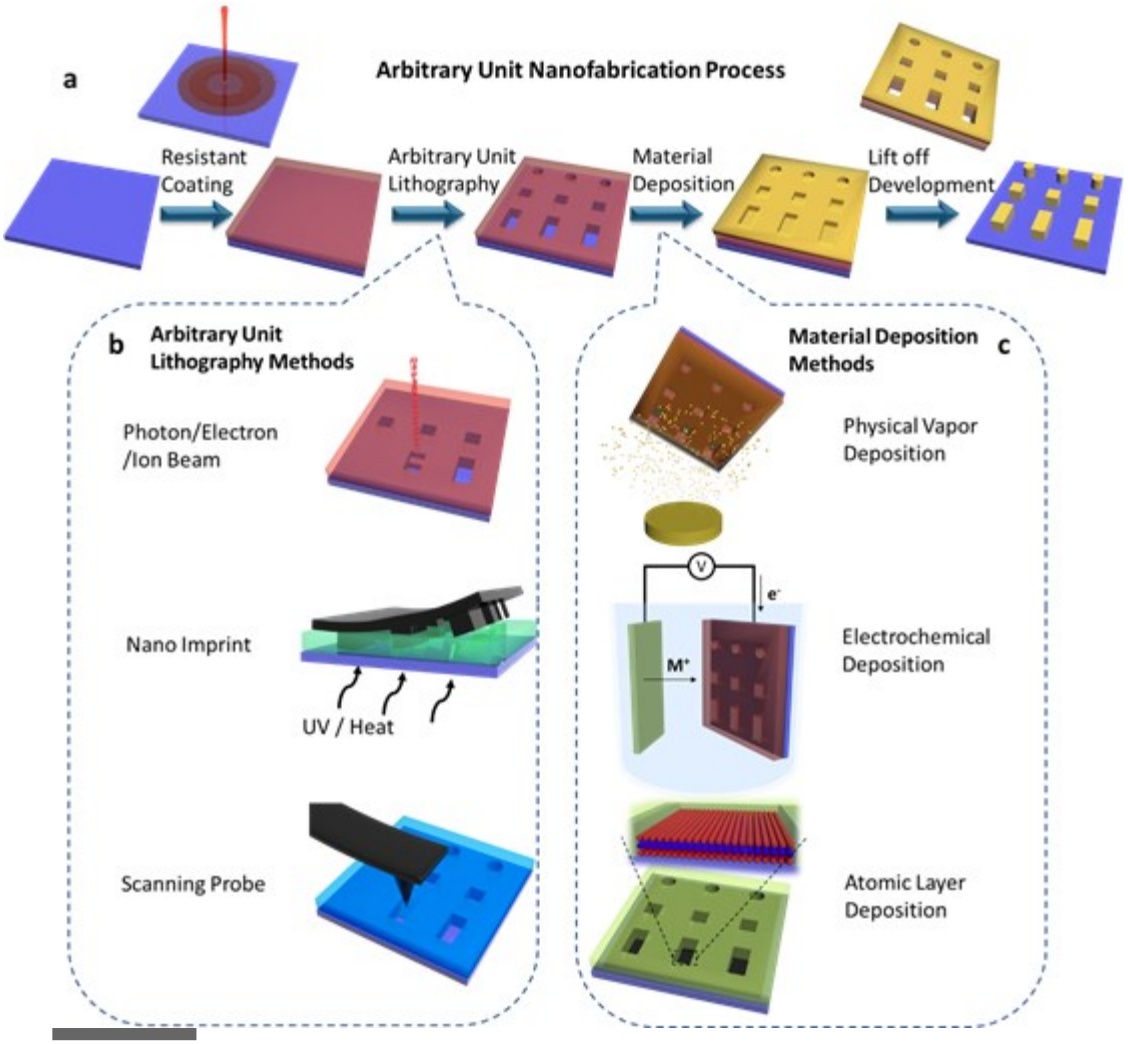

Figure 1. Fabrication of arbitrary nano-unit arrays. (a) Schematic of the general fabrication process. (b) Examples of three commonly used nanolithography techniques. (c) Examples of three commonly used material deposition methods.

In this section, we introduce the process of arbitrary unit nanofabrication, which combines multiple (well-established) steps including resist coating, pattern lithography, nanostructure deposition, and post-fabrication development (figure 1a). We will focus mainly on the developments around pattern lithography methods and nanomaterial deposition.

Top-down lithographic tools are normally used to generate the mold of the nano unit by applying energy to change or break the structure of the resist coating, as illustrated in Figure 1b. While photolithography is widely used to form microstructures and alignment markers, it is not suitable for generating accurate patterns at the nanoscale. In order to achieve sub-100 nm features, electron or (Ga, He) ion beams are normally used, and with cutting edge, electron beam lithography (EBL) tools it is now possible to obtain a spatial resolution of less than 10 nm.[6a, 15] However, EBL requires sophisticated and expensive equipment and it is a relatively slow process for large scale patterning. For example, in our experiments, a 6 cm^2 area containing 50 nm features requires around 5 h of EBL time, not including resist

development. Nevertheless, it is invaluable as a primary prototyping method due to its high reproducibility and resolution.

Nanoimprint lithography (NIL) overcomes the limited scalability of EBL-based techniques.[16] NIL is a secondary fabrication technique, whereby the template is transferred from a master stamp to a substrate, as shown in Figure 1b. The master stamp is normally fabricated by EBL with designed concave-convex structures in a relatively hard material. This master is then used to stamp the pattern into a thin film of a curable polymer by applying pressure. Finally, the master stamp is removed after the imprinted pattern is fixed by photo- or thermal curing of the polymer.[17] A large number of nanostructures can be fabricated rapidly and simultaneously. In addition, NIL can be readily adapted to roll-to-roll processes, thus overcoming the inherent scalability issues with EBL.[18] One concern with NIL, particularly for single nanocrystal deposition, is that due to the nature of the stamping process, residual resist will often be left at the bottom of imprinted nanostructures, which complicates a number of the assembly methods that we describe later in this review.

Scanning probe lithography (SPL) provides another approach to the generation of nanoscale features. The basic idea behind SPL is to induce changes to the coating layer using the scanning probe tip.[19] This probe alters the coating resist through the application of thermal, mechanical, or chemical interactions with the substrate. For example, heated probes can be used to selectively induce local oxidation of the substrate, and these regions then act as binding sites for nanocrystals. Alternatively, the probe can carry chemical species that are deposited onto the substrate when in contact – termed dip-pen SPL.[20] SPL opens up the ability to fabricate inclined structures and thus generate nanostructures in greyscale – something very challenging to achieve via EBL.[21] Like EBL, SPL is a process where the nanostructures are patterned in a serial manner and thus the technique cannot be readily scaled up. However, patterns generated by SPL can be transferred via etching to a substrate for use in NIL, thus allowing directed nanocrystal assembly to be prototyped with EBL or SPL templates and then scaled up via NIL.

2.2 Top-down deposition

To fabricate the desired nanocrystal arrays, the material is often deposited across the entire template via a top-down process such as physical vapor deposition (PVD) as shown in Figure 1c, followed by lift-off of the underlying resist to leave only the nanostructures on the substrate. In one instance of PVD, the target material is evaporated under ultrahigh vacuum by heating the target material with a large current, or by heating with an electron beam. The vapor then deposits and solidifies on the surface of the substrate with nanometer thickness control. Many metals and a large number of alloys and metal oxides have been successfully deposited by PVD methods.[22] However, the choice of binary materials and molecular compounds is still comparatively limited and there is also little potential for creating more complicated 3D nanostructures. Additionally, there is poor control over the crystallinity of

deposited materials and most metal structures are polycrystalline while most metal oxide layers are amorphous.

Another deposition method, which has far lower production costs, is electrochemical deposition (ECD). The basic principle of ECD is to flow an electric current through a conductive substrate, which reduces ionic species in solution or oxidizes the substrate or reduced material in solution, leading to nucleation and growth of material on the substrate.[23] ECD is used in many industry fields for large scale surface coating or plating. Combining this with nanostructured lithography, ECD method has been developed into an effective and convenient method for the scalable deposition of nanostructures.[24] However, as with PVD, the choice of materials in ECD is limited due to the range of dissolvable precursors. It is also challenging to control the crystallinity and quality of the deposited nano-unit.

Recently, atomic layer deposition (ALD) has become a widely used technique for the fabrication of complex nanostructures. ALD constructs materials conformally on surfaces by sequential injection of a first precursor into a vacuum chamber that reacts with the substrate in a self-terminating fashion followed by injection of a second reactive precursor.[25] This builds up thin films one atomic layer at a time. A major advantage of ALD is the excellent, ultra-thin, conformal coating it generates, i.e. pin-hole free, as well as the wide range of available materials and reasonable control over crystallinity. One complicating factor is that the precursor will often react with both the substrate and any resist. Hence the chemistry of the resist needs to be considered. In some cases, the ALD precursors can be deliberately designed to convert the resist into other compounds, termed sequential infiltration synthesis.[26]

2.3 Applications of fabricated nanostructures

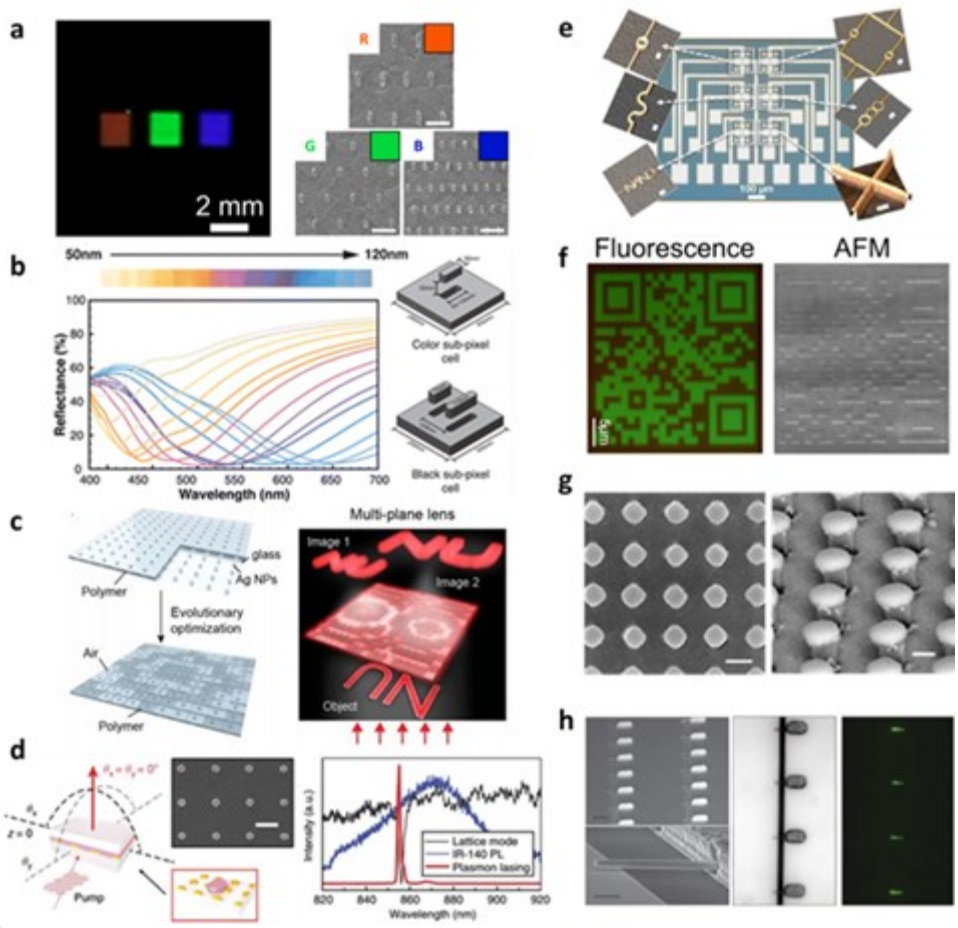

Figure 2. Current development and applications derived from arbitrary unit nanofabrication. (a) EBL lithography patterned aluminum nanocrystal arrays with different periodicity orders. The varied spacing leads to different coupling across the arrays and results in a full-RGB plasmonic pixel. Adapted with permission.[27] Copyright 2015, American Chemical Society (b) EBL patterned and EBE deposition of aluminum nanostructures for fabrication of a polarization-sensitive plasmonic pixel in CMYK. Adapted with permission.[28] Copyright 2016, American Chemical Society. (c) Photolithography patterned silver nanoparticles arrays selectively embedded in polymers. By tuning the air-polymer patterning, the array can function as a single-focus lens or even multi-plane lens. Adapted with permission.[29] Copyright 2019, American Chemical Society (d) Photolithography patterned gold nanoparticle arrays fabricated as a lasing device. A sharp and narrow emission is generated when the IR-140 dye emission overlaps with lattice plasmon resonances of the gold nanoparticle array. Adapted under the terms of the CC BY license.[30] Copyright 2015, Nature Publishing Group. (e) Oxidative SPL patterned silicon microcircuit. The flexibility of SPL allows complex patterned structures to be realized. Adapted with permission.[6c] Copyright 2010, Institute of Physics. (f) Thermal SPL generated fluorescence pattern and corresponding AFM characterization. Adapted under the terms of the ACS AuthorChoice license.[31] Copyright 2017, American Chemical Society. (g) Thermally evaporated gold mushroom arrays as refractive index sensors with high figures of merit. The array structure gives rise to a strong and sharp Fano resonance and increases the refractive index sensitivity. Adapted with permission.[32] Copyright 2013, Nature Publishing Group. (h) Electric field and electrochemically deposited silicon and rhodium nanowires clamped by a gold electrode. The nanowires were coated with peptide nucleic acid probe sequences for hepatitis C detection. Adapted with permission.[33] Copyright 2008, Nature Publishing Group.

The goal of nanofabrication is to open up new applications that can be achieved only through structuring with nanometer resolution. This includes fabrication of plasmonic structures, quantized fluorescent nanostructures, and structural materials which exhibit chiral color.[34] Nanofabrication is also widely used for advanced electronics and novel sensing devices.[35] Most of these applications have been reviewed elsewhere. Here, we selective a few representative examples to briefly introduce the applications of nanofabrication.

One area where single nanocrystal assembly is gaining importance is the design and construction of materials with structural color. For example, researchers often couple the plasmonic properties of metallic nanocrystals with periodic metamaterials to generate new and interesting optical effects.[34c] In order to achieve this coupling, highly accurate fabrication tools are needed to ensure the plasmonic resonances of individual elements in the array are suitably narrow.[36] In 2015, Olson et al. reported the fabrication of high-chromaticity, aluminum plasmonic pixels in RGB color, composed of individual aluminum nanorods, fabricated by EBL and electron-beam evaporation of the aluminum through the resist mask, as shown in Figure 2a.[27] In 2016, James et al. reported the fabrication of a plasmonic pixel based image exhibiting CMYK gamut colors over large areas by arranging aluminum nanoparticles in a Babinet screen structure as shown in Figure 2b.[28] Both EBL and NIL were demonstrated to be effective methods for plasmonic pixel fabrication meaning this is a scalable approach for formation of materials with structural color. The efficacy of these plasmonic pixels relies on the generation of highly reproducible and accurate resist masks. In addition, another important group of nanofabricated structures are helical metamaterials.[34d, 37] These are mainly fabricated through top-down fabrication methods or via DNA-assisted assembly methods. The resulting structures exhibit strong, structurally dependent chiral optical properties and these can be used as chiral nanoresonators[38] and asymmetric optics.[39] While most plasmonic metals can be deposited via PVD, fabrication of more complex core-shell structures, single crystal nanocrystals, and plasmonic metal oxides still necessitates the use of colloid synthesis. Therefore, we expect even more plasmonic pixel architectures could be fabricated by combining EBL/NIL of masks with bottom-up assembly of these plasmonic nanocrystals.

The manufacture of optical devices such as nanoantennas,[40] metalenses,[29] and lasing devices.[30] has been widely impacted by the development of nanofabrication methods. The accuracy of the nanofabrication tools, the choice of material, and the quality of the nanofabrication all significantly affect the resultant properties of the final optical device. A typical example is the manufacture of metalenses for optical imaging, as shown by Hu et al., who reported such reconfigurable meta-lenses (figure 2c).[29] These were fabricated by photolithography on a PDMS mask followed by PVD of 50 nm Au and Ag nanoparticles. The surface lattice resonances of coupled nanoparticle arrays were tuned by altering the local refractive index on each nanoparticle, leading to optical phase and intensity differences. The resulting pattern enabled production of images in multiple planes for 3D and multifocal imaging. A recent type of optical device that has attracted much attention is that of coupled plasmonic lasers. Yong et al. reported a refractive index sensitive, real-time tunable plasmonic lasing system via nanofabrication of Au nanoparticles (figure 2d).[30] The device

was fabricated by photolithography of a mask followed by PVD of plasmonic metals combined with IR-140 dye molecules. Due to the plasmon-exciton energy transfer between lattice modes of the nanoparticle array and excitation of the molecular dye, a sharp and intense emission was generated.

Nanoelectronics, as a field, has rapidly expanded with applications beyond computing such as information storage, optoelectronics, and biosensing.[19a, 20, 41] One of the main challenges for the construction of nanoelectronic devices is the ability to precisely fabricate various materials (not only semiconductors) at the nanoscale with a high degree of structural flexibility. Scanning probe lithography is one technique that can help to address this challenge. SPL is a robust and flexible probe-driven fabrication method that enables nanomaterials to be "written" on demand. Martinez et al. reported SPL-based oxidative fabrication of silicon nanowires with 10-20 nm channel widths transistors (figure 2e).[6c] In their study, a biased SPL probe locally oxidized a silicon-on-insulator substrate thus forming an oxide mask with sub 20 nm resolution, resulting in thin silicon wires after etching. Besides this, SPL can also induce intermolecular changes for patterning of materials other than semiconductors. Zimmermann et al. reported the use of SPL to pattern fluorescent polymers by selectively quenching the fluorescent polymer with heat (figure 2f).[31] These fluorescence patterns were used to write QR codes as shown in figure 2f, and this concept can be easily extended to the nanoscale for generation of latent (hidden) optical features.

An important justification for single nanocrystal arrays is the burgeoning demand for new sensing technologies with the potential to solve global challenges in health. As part of this demand, a sensing technology should possess good sensitivity, fast response time and high biomolecular selectivity.[42] As an example of how nanofabrication can help achieve this goal, Shen et al. reported the fabrication of mushroom-like gold nanostructures as transducing elements by photolithography followed by PVD (figure 2g).[32] The coupling between closely packed array elements and the mushroom morphology greatly enhanced the plasmonic response of the device. The resulting reflection spectrum of the array is very sensitive to changes in the local refractive index resulting from the binding of targets. In another example, Li et al. reported the fabrication of nanowire arrays for hepatitis C detection by photolithography and ECD (figure 2h).[33] The nanowires were functionalized with peptide nucleic acid probe molecules and suspended above a gold thin film and clamped with a gold electrode. The nanowire and Au thin film formed a resonator system. When the nanowire array was exposed to a fluorescently labeled oligonucleotide, complementary to the hepatitis C probes, a fluorescence signal was observed on each of the nanowires. This approach allowed an improvement in the selectivity and sensitivity of hepatitis C detection due to the fabrication of an array of resonators with individual analytics on each of the single resonator units. It also demonstrated the potential for arrays of selectively functionalized nanocrystals to sense a multitude of targets on each of the nano units.\

2.4 The Challenges and Opportunities of Nano Fabrication in Nanotechnology

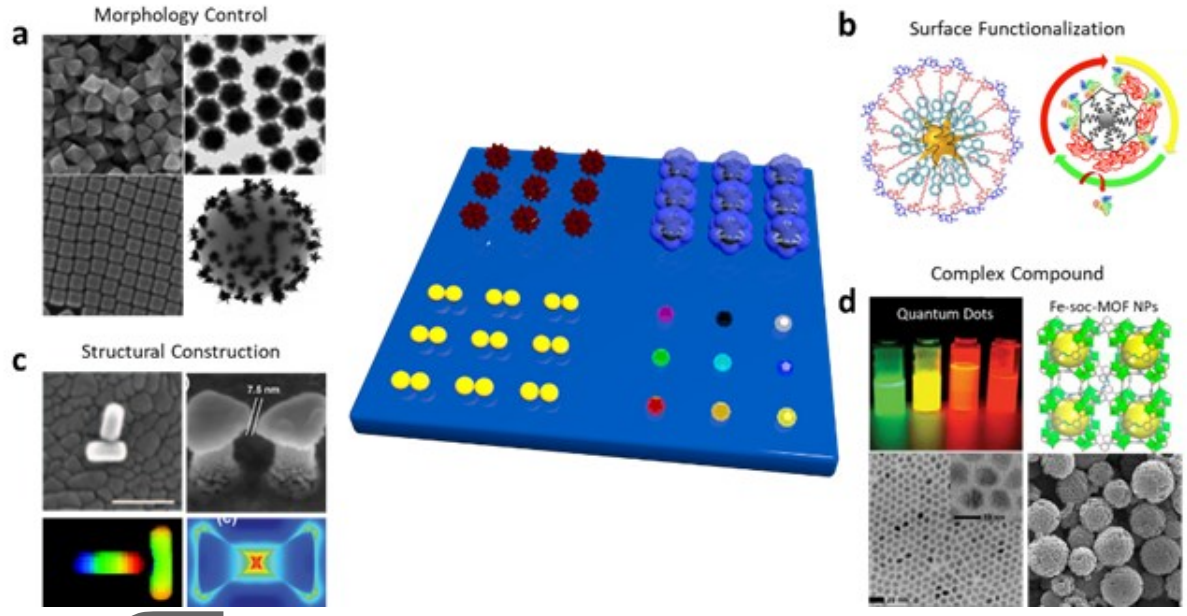

Figure 3. Challenges and opportunities for current arbitrary nanofabrication. The schematic image in the middle shows four types of potential arrays that are challenging to fabricate by conventional nanofabrication methods. In turn these are: (a) Assembly of nanocrystals arrays with controlled morphology. Adapted with permission.[43] Copyright 2008, American Chemical Society. Adapted with permission.[44] Copyright 2013, The Royal Society of Chemistry. Adapted with permission.[45] Copyright 2016, Wiley-VCH. Adapted with permission.[46] Copyright 2016, American Chemical Society. (b) Assembly of surface functionalized nanoparticles arrays. Adapted with permission.[47] Copyright 2016, American Chemical Society. Adapted with permission.[48] Copyright 2015, American Chemical Society. (c) Assembly of arrays with complex morphologies. Adapted with permission.[49] Copyright 2009, American Chemical Society. Adapted with permission.[50] Copyright 2010, American Chemical Society. (d) Assembly of arrays of nanoparticles with complex internal structure e.g. core-shell nanocrystals. Adapted with permission.[51] Copyright 2013, American Chemical Society. Adapted with permission.[52] Copyright 2013, American Chemical Society.

As summarized above, both lithography and material deposition techniques are necessary components in the process of arbitrary unit nanofabrication. Each has specific advantages and limitations, with different techniques chosen as needed. However, challenges remain with the use of techniques described so far, and consequently there are opportunities for development in this area.

Challenge 1: To fabricate arrays of single nanocrystals with complex morphologies.

With current lithography methods, it is nearly impossible to fabricate nano-units with complex structures such as ultra-smooth spheres,[53] polyhedrons,[43-44] nanostars,[45, 47] or core-shell particles.[54] These nanocrystals have desirable physical and chemical properties. For example, the gold nanostars shown in figure 3a exhibit extremely high Raman scattering intensities but cannot be created by conventional top-down processing and deposition.

Challenge 2: To assemble pre-functionalized single nanocrystals.

Nanocrystals with controlled surface functionalization are widely used as selective sensing elements.[47-48, 55] Typically, these materials are randomly deposited onto substrates and studied as a random ensemble. If a controlled array of these surface-functionalized nanocrystals could be fabricated, then each unit could be individually addressed and, if they possessed various chemistries, they could be massively multiplexed. However, conventional deposition methods limit the possibility to achieve this.

Challenge 3: To assemble single nanocrystal patterns as demanded in multiple dimensions.

Coupling between nanocrystals often leads to the rise of new exotic properties that are challenging to achieve with a single nanocrystal. This coupling effect between particles is highly dependent on how the coupling units are constructed[49], such as the coupling distance between particles,[36] the geometry of the building blocks,[12] and the materials they are constructed from. However, most reports on nanocrystal coupling have been limited to two-dimensional, (in-plane) coupled systems. Therefore, there is an opportunity to develop other nanofabrication tools to scalably and reproducibly generate coupled nanostructures in three dimensions.

Challenge 4: To assemble nanocrystals of any material or composite.

Top-down processes are limited in terms of the materials that can be deposited. However, nanocrystals have been synthesized from the majority of elements of the periodic table and in a plethora of combinations. Depending on their composition, size, and molecular structure, they can exhibit outstanding and unique properties. For example, cadmium selenide (CdSe) nanocrystals [51] exhibit size-dependent, high quantum yield luminescence but this effect cannot be reproduced using top-down deposition. Metal-organic-frameworks (MOF) are also promising materials that could benefit greatly from inclusion into nanofabricated devices.[52, 56] With nanofabrication, MOF nanoparticles can enable further progress in catalysis,[57] energy storage,[58] and targeted bio-absorption.[59] Again, these materials, in their most efficacious form, cannot be deposited via conventional, top-down PVD tools.

In summary, we have shown in the above sections that while modern lithography tools offer arbitrary ***design*** of nanostructures, current top-down deposition techniques are limited to a small range of materials and the challenges outlined above do not seem to be solvable via current methods. Instead nanofabrication approaches are required which enable the direct assembly of pre-synthesized single nanocrystals. These nanocrystals can be fabricated from many elements and should be deposited in a controllable process with nanometer precision, be compatible with 3D structure development, and have the potential for scale up. Directed, single nanocrystal assembly is one of the best approaches to achieve these goals.

3. Directed Assembly

3.1 The principle of directed assembly of nanocrystal arrays

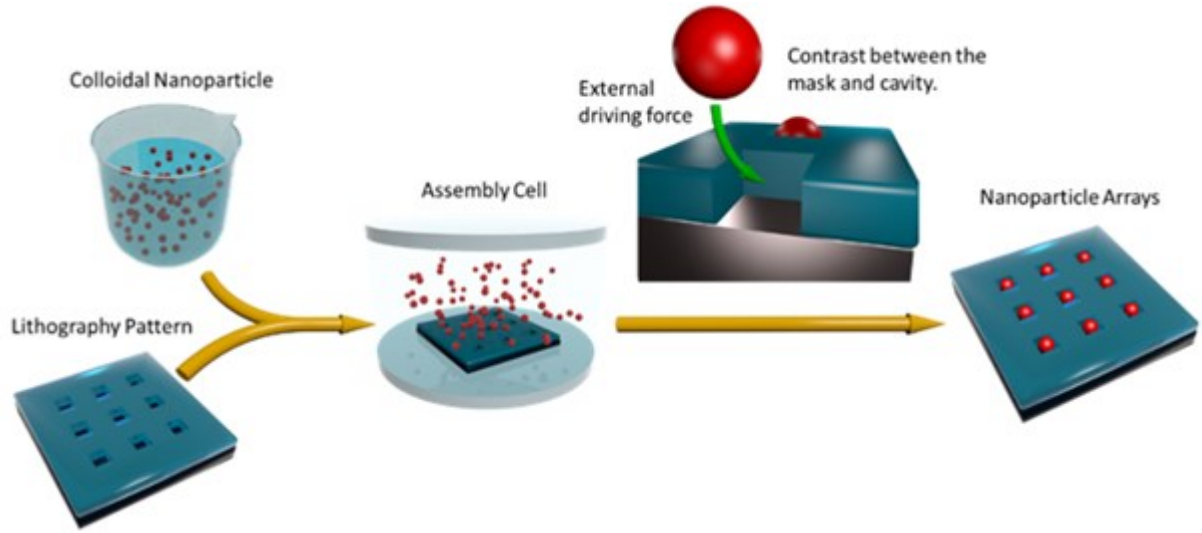

Figure 4: Overview of directed assembly processing. The wet-chemically-synthesized nanocrystals and lithographically patterned templates are assembled together in a cell. To achieve nanocrystal assembly, an external force is required to drive the nanocrystals to deposit on the template. To achieve selective deposition into the wells, physical or chemical or biological contrast between the wells and the resist is required.

Directed assembly is a method to assemble pre-synthesized nanomaterials onto a pre-patterned substrate by application of an external force. The morphology and properties of the nanomaterials should be preserved after the assembly. The most important factor for practical directed assembly is the selection of the proper external force (Figure 4).[35] In addition, developments in lithography tools, as discussed previously, provide the possibility to arbitrarily pattern templates with high resolution. To combine the colloidally synthesized nanomaterials with patterned templates, a cell is usually required to ensure reproducible assembly. The external force needs to fulfill the following requirements: 1) It needs to induce an interaction between the substrate and nanoparticle with sufficiently different contrast to the resist/substrate. 2) It needs to have enough strength to overcome Brownian motion, particle-substrate repulsion, and particle-particle interactions. 3) It needs to be a force that can be modulated so that the assembly parameters can be optimized according to the target nanocrystal's shape and size and it must be able to accommodate differences in the pattern structure on the substrate. 4) To be scalable, any method must be able to assemble single nanocrystals extremely quickly in a serial manner or to act across the entire ensemble of nanocrystals in parallel. There are several promising external forces which we assess in the following sections.

3.2 Capillary Force Assembly

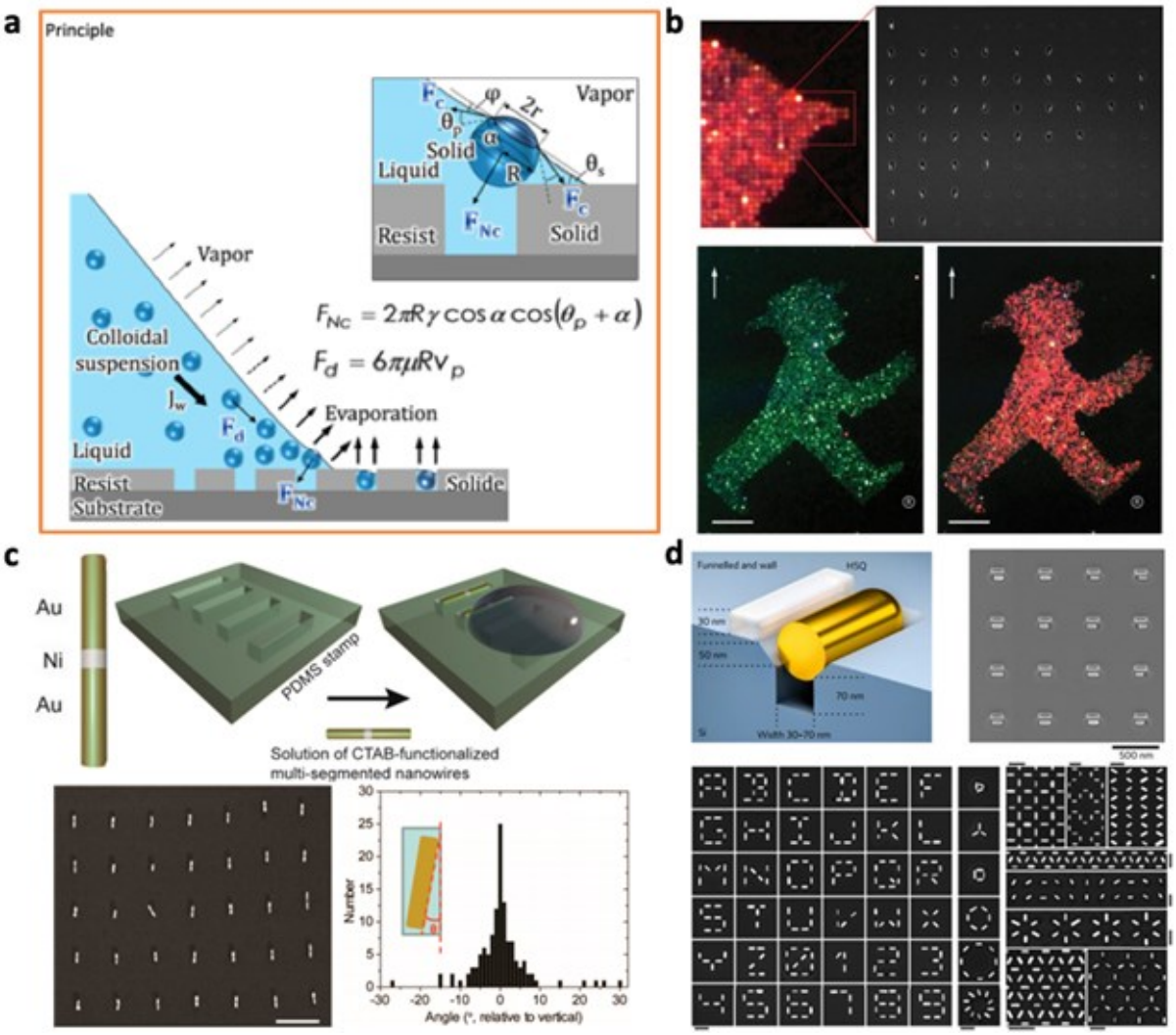

Figure 5: Overview of capillary force assembly (CFA). (a) A nanopatterned resist is created by FIB or EBL. Passive evaporation of the solvent leads to the steady migration of the three-phase contact line over the template. The dynamic, receding contact angle leads to a residual downward tension that drives particles into the cavities.[60]. (b) Assembly of gold nanorods into rectangular cavities by CFA. The array exhibits excellent cavity-dependent, orientation properties. Adapted with permission.[61] Copyright 2012, Wiley-VCH. (c) CFA of gold-nickel-gold nanowires arrays. This assembly also shows excellent cavity-dependent orientation and the approach has been extended to other nanomaterials. Adapted with permission.[62] Copyright 2014, American Chemical Society. (d) Assembly of nearly perfect oriented gold nanorod arrays by capillary force assembly. The funnel shaped cavity and well were designed to improve the degree of alignment of the gold nanorods within the cavities. Adapted with permission.[63] Copyright 2017, Nature Publishing Group

One of the most studied methods for alignment and assembly of discrete, single nanoscale objects is capillary based assembly. The principles of this process are outlined in Figure 5.[64] A template is prepared, consisting of a PMMA coated substrate, in which wells are constructed by EBL followed by development of the PMMA. The wells are usually designed to accommodate a single nanocrystal of a particular shape. The resolution and quality are therefore limited primarily by the EBL tool and particles down to 10-20 nm in diameter can be assembled. A solution of the nanocrystals is applied to the template and drawn over the

surface by two methods. In the first case, the solvent simply evaporates while in the second it is actively drawn across the surface. At the three-phase contact line, there is a residual downward force due to surface tension that acts to push particles into the cavities. By controlling the speed of the interface and the contact angle, the template may be almost quantitatively filled. The capillary assembly method has been applied to a number of micron scale particles such as latex[65], as well as gold nanospheres[60a] and gold nanorods.[61, 66] There is also excellent control over the numbers or arrangements of nanocrystals placed into each unit cell, this can range from single nanocrystals up to close-packed superstructures.[67] Of particular importance is that the assembly force can be applied to a wide range of nanocrystals: inorganic, organic, or hybrid, as well as to nanocrystals with different shapes and sizes. It has been successfully used to orient particles on surfaces as well,[62] as shown in Figure 5.

While it is an attractive method, in practice CFA has a number of critical drawbacks that have prevented large scale implementation. Firstly, the range of contact angles that yield high filling fractions is quite small, usually around 40-45 degrees. This is a function of the surface tension of the wetting liquid. Hence the choice of particle, substrate (PMMA) and solvent must be chosen carefully. Both complete wetting (contact angle < 10°) and non-wetting (contact angle > 80°) do not allow efficacious deposition. In many cases water has been used since its contact angle with PMMA is close to the desired range. The PMMA can be made more or less wetting by plasma treatment or chemical oxidation, or by adsorption of a thin polymer layer. However, the contact angle is highly sensitive to the presence of surfactants and polymers, which both reduce the solvent-air surface tension. Considerable effort to purify nanocrystal solutions is therefore needed in order to maintain a reproducible interfacial tension. A bigger drawback is capillary pinning. Depending on the exact profile of the cavity rims, the three-phase contact line can readily become pinned on cavities. This is also exacerbated by any impurity (e.g. dust) on the surface or surface roughness from the initial lithography. Under these circumstances, the contact line becomes pinned, while the main solvent front continues to recede across the surface. The solvent interface near the pinned region then jumps, often tens of microns in order to restore the contact line, resulting in large areas of unfilled cavities. Scale up has been a major impediment for this method.

Source	Contact Angle	Contact Line Speed	Maximum Array Area	Minimum Inter-Cavity Spacing
Cui et al.[68]	10° to 30°	Not stated	100 × 100 μm^2	1 μm
Pinedo-Rivera et al.[60a]	24° to 37°	1.7 to 3.3 μm/s	Not stated	2 μm
Pinedo-Rivera et al.[60b]	30°	~1 to 3 μm/s)	Not stated	4 μm
Kuemin et al.[66]	56°	2 μm/s	~ 80 × 80 μm^2	1 μm
Fan et al.[69]	25°	0.6 μm/s	Not stated	2 μm
Rey et al.[70]	50°	0.1 μm/s	Not stated	Not stated
Kuemin et al.[61]	35°	0.5 to 1 μm/s	50 × 60 μm^2	500 nm
Kraus et al.[71]	50° to 60°	0.3 μm/s	~ 80 × 80 μm^2	280 nm
Liddle et al.[72]	10° to 30°	0.17 μm/s	Not stated	1 μm
Gordon and Peyrade[73]	Not stated	0.1 to 2 μm/s	100 × 100 μm^2	850 nm
Malaquin et al.[71]	30° to 60°	0.2 to 10 μm/s	Not stated	100 nm
Mehraeen et al.[74]	12°	1.7, 5 and 17 μm/s	N/A	N/A
Asbahi et al.[75]	12°	10 μm/s	5.4 × 4 μm^2	27 nm

Table 1.1: Table of relevant published nano-CFA experimental parameters.

Table 1.1 lists some of the works where all the relevant parameters can be extracted from the CFA experiments. It shows that deposition speeds of 1-100 μm/s are most efficacious but that areas larger than a few 100 μm^2 are difficult to achieve. Although individual cavities may be down to 20 nm in diameter, the cavities need to be spaced quite far apart (> 1 μm) for quantitative filling. High density assembly is not possible due to the difficulty of obtaining the necessary curvature of the contact line.

The theory of CFA is still in its infancy. Double layer interactions between the particles and between the particles and the substrate are not included in the current models. Furthermore, hydrodynamic effects that occur as the particle displaces the solvent in the well have been neglected thus far, while Marangoni effects at the contact line due to the rapid changes in surfactant and salt concentrations have also not been incorporated into modelling to date. However, progress in improving the deposition efficiency using more elaborate, funnel-shaped cavities has been reported (see Figure 5d). A further challenge is understanding the transition between single particle filling and multiple particle filling. It will be extremely useful to be able to generate well-defined clusters in these arrays as demonstrated by Mapperson but this process has not been modelled to date. Mapperson has also argued that the receding contact angle is poorly defined in these dynamic systems and needs to be determined for each individual system under study.[64]

3.3 Electrostatic Assembly

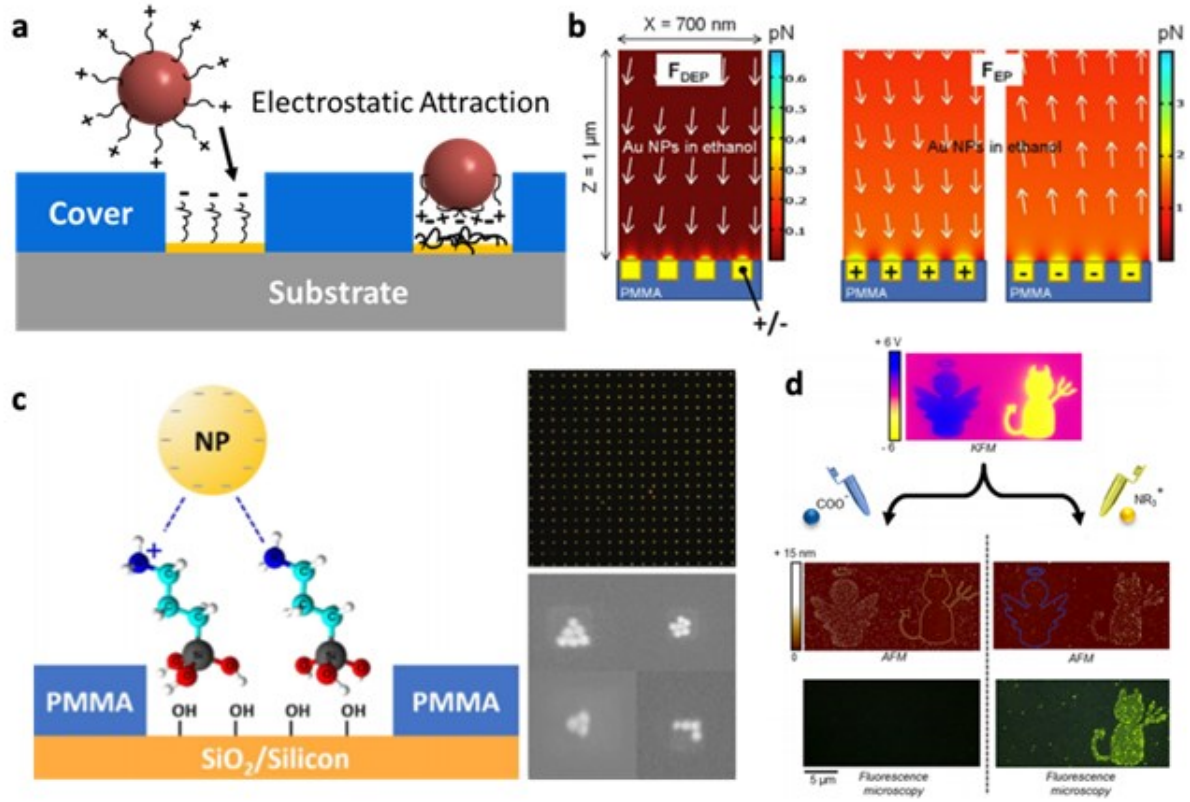

Figure 6: Summary of electrostatic assembly. (a) Schematic image to illustrate the principle of electrostatic assembly. The nanoparticle is firstly functionalized with ionic charges, typically through ligand adsorption. Then the substrate cavity is functionalized with the complementary charge. Finally, it is useful where possible to ensure the PMMA substrate has the same surface charge as the nanocrystals. Due to the electrostatic attraction between the nanoparticle and the cavities, and the surface charge contrast between the PMMA and the nanocrystals, the nanoparticle will preferentially diffuse (migrate) to the cavities and will adsorb within the cavities. (b) Numerical simulations for the force fields acting during deposition of gold nanocrystals in ethanol. Reproduced with permission.[76] Copyright 2011, Institute of Physics. (c) An array of gold nanoparticles assembled by electrostatic forces. The surfaces of the gold nanoparticles were functionalized with negatively charged bis(p-sulfonatophenyl) phenylphosphine (BSPP) while the surface of the silica substrate was functionalized with positive charges by salinization with aminopropytriethoxysilane. Reproduced with permission [77] Copyright 2018, American Chemical Society. (d) Binary, electrostatic assembly of nanogels. The substrate pattern was made by depositing either positive or negative charges via Kelvin force microscopy (KFM). Nanogels with different functional groups (carboxylic groups for negative charge, amide moieties for positive charge) could be selectively assembled. Reproduced with permission [78] Copyright 2018, American Chemical Society.

The first use of patterned electrostatic charges to print oppositely charged particles dates back to 1938 when xerography, originally coined electrophotography, was invented by Chester Carlson.[79] In this process, charge contrast on a photoconductive surface was generated by illumination through a negative mask (i.e. the document to be copied), and this surface then attracted the dry toner particles. Here, we consider the liquid-phase equivalent, where a

patterned surface charge is used to attract oppositely charged nanocrystals in suspension, as shown in Figure 6a.

Electrostatic charges can be immobilized on the surface of, or trapped within, a substrate by various methods. One of the earliest applications used short voltage pulses between a conductive atomic force microscopy (AFM) probe and an insulating substrate to locally deposit electrical charge, positive or negative.[80] These charges can be immobilized in insulators such as PMMA,[80] sapphire crystals,[80] native oxides on silicon,[81] and PTFE,[82] among others. This is commonly referred to as AFM nanoxerography and can be performed in parallel using electrode stamps, inspired by microcontact printing soft lithography.[83] While the resolution of these stamps is limited by the standard of the lithographic technique used to make them, advances in focused particle beam technologies suggest this is a promising route to high resolution arrays of single nanocrystals.[84]

An alternative process is to use conventional lithography to fabricate a pattern with some form of chemical contrast, and then to selectively functionalize the pattern with charged functional groups. As an example, aminopropyltriethoxysilane has been used to functionalize a silicon oxide surface. Patterned PMMA films provided the electrostatic contrast.[77] Alternatively, AFM probes can be used to selectively oxidize the surface of a silicon wafer which provides electrostatic contrast with high resolution – sufficient to assembly single ferritin molecules in rows.[85] In another example, polylysine was shown to preferentially bind to a glass substrate coated with a PMMA mask providing binding sites for negatively charged nanocrystals in suspension.[86]

A number of requirements must be met for high-resolution, deterministic single nanocrystal assembly. 1) The patterned charges should be deposited with high spatial resolution, ideally similar to the size of the material being deposited. Note the effective size in solution includes the double layer thickness (i.e. Debye length), and the surface charges need to be relatively immobile. 2) The dielectric strength of the suspending media should be high enough to ensure the electrical fields on adjacent patches of surface-bound electrical charges do not significantly overlap. 3) The nanocrystals need to carry sufficient charge to overcome Brownian motion and deposit on the patterned substrates. 4) There should be enough repulsion between the suspended nanocrystals and the background substrate to avoid non-specific deposition.

Kinnear et al. recently demonstrated electrostatic assembly where an SiO_2 surface was functionalized with amine groups and patterned with PMMA via EBL (Figure 6c).[77] The PMMA film bore a slight negative charge in the aqueous media and thus high electrostatic contrast was generated between the background and the pattern enabling the deposition of single or clusters of negatively charged gold nanocrystals, from 10 to 120 nm. Addition of salt screened both the interparticle electrostatic repulsion and the repulsion from the PMMA thus leading to clusters of spheres depositing within each pattern. In a similar approach, electrostatic focusing has been shown to work for silver and gold nanocrystal aerosols, and deposition with extremely high resolution was achieved when there was differential charging between the photoresist and electrode.[87] The concept of focusing also applies to planar

electrostatic patterns where single negatively-charged gold nanorods were assembled onto positive stripes of polymer despite the pattern being large enough to accommodate more than one nanorod.[88] In this example, repulsion between neighboring rods, through control of the ionic strength, was used to alter the number of printed rods per stripe.

Highly localized and immobilized charges can also be readily obtained by AFM nanoxerography. As shown in Figure 6d, Ressier and coworkers used nanoxerography to write various images on a PMMA film, which were then developed when exposed to cationic or anionic pNIPAM nanoparticles.[78] In this example, nanoxerography was used to attract clusters of nanoparticles in order to detect hidden patterns in a concentration-dependent encryption method. However, if the charges are written with the highest possible resolution, then single nanocrystals can be adsorbed. In an earlier paper, Ressier et al. showed this by writing lines comprising single charge dots, which act as anchor points for the adsorption of slightly negatively charged gold nanowires in hexane.[89] Lines composed of dots spaced 200 nm apart written with either +70 V or +55 V pulses led to deposition of linear bundles of gold nanowires. However, when the voltage pulses were decreased to +30 V and spaced 50 nm apart, they observed deposition of a single gold nanowire, only 1.7 nm in diameter, elongated along the line of charged dots proving that even the smallest of nanocrystals can be electrostatically printed with extremely high resolution. While this works well for AFM-based nanoxerography, as well as surface charging with electron beams or ion beams,[84, 90] the scalable equivalent, electrical NIL, is still limited by the large size of the stamps used to transfer charge.[83b, 83d, 83e, 91] We are not aware of any example in the literature where a scalable nanoxerography approach has been used to assembly single, sub 50 nm nanocrystals from suspension.

3.4 Optical printing

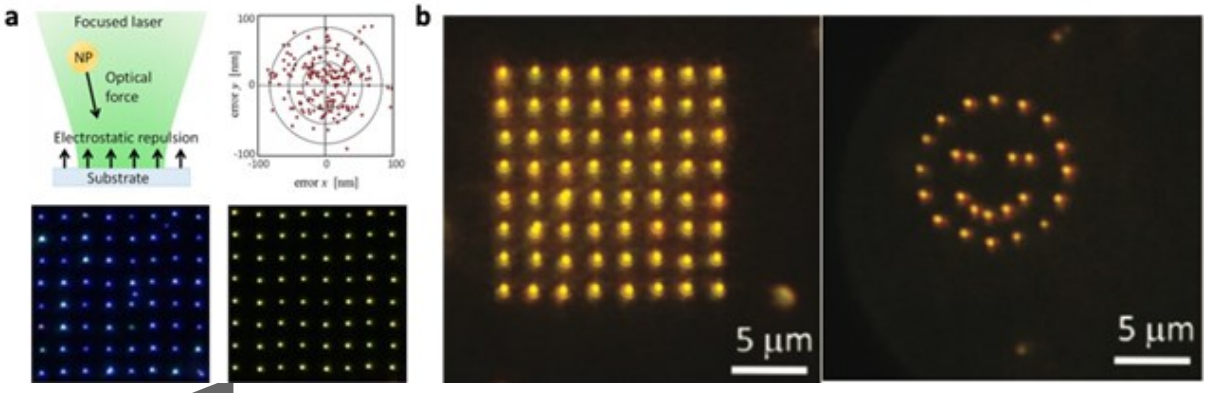

Figure 7: Summary of optical printing of single nanocrystals. (a) Optical printing of single gold and silver nanoparticles. A focused laser was used to guide and drive the nanoparticle to deposited onto the surface. Reproduced with permission.[92] Copyright 2017, American Chemical Society. (b) A 8 × 8 array (left) and a "smiley face" (right) pattern assembled with single 80 nm gold nanoparticles. Reproduced with permission.[93] Copyright 2011, American Chemical Society.

In addition to electrostatics and convective-capillary forces, the electromagnetic fields generated from tightly focused laser light enable trapping and printing of single nanocrystals with high precision and accuracy – this process is termed optical printing. The Nobel Prize in Physics for 2018 was awarded for work in the field of laser physics, in part for the development of optical tweezers. While this technique was widely used for trapping dielectric microparticles and cells, it was discovered in 1994 that it could also be utilized to trap sub-wavelength sized metallic nanocrystals. [94] The physical mechanism behind this phenomenon has been well described in other reviews.[95]. Laser printing of single nanocrystals is carried out by first trapping them, and then using the radiation pressure of the trap to direct them close to a substrate where van der Waals forces take over and irreversibly bind the nanocrystal to the surface, as shown in Figure 7a. Urban et al. used this phenomenon to laser print 80 nm gold nanocrystals with a cationic polyelectrolyte (pDADMAC) onto a positively charged surface with 50 nm precision, at a rate of roughly 5 s per particle.[96] They found that the printing precision was affected by laser-induced heating, Brownian motion, and the ratio of axial (towards the substrate) to radial (towards the center of the optical trap) forces in the optical trap. Gargiulo et al. recently studied these effects for 60 nm Au and Ag nanocrystals and found similar levels of precision with radial standard deviations of around 38 nm. This was independent of laser polarization and resulted in a printing time of around 5 s per nanocrystal.[92a] They also described the role of illuminating on or off-resonance: on-resonance provided high resolution printing only at low powers, whereas the precision was slightly poorer off-resonance and independent of the laser power.[92a]

Laser printing has also been used to print Au and Ag nanocrystals in close proximity to one another, as long as their LSPRs are offset.[97] When there is no offset, the focused laser heats up the nanocrystal printed first, which leads to thermophoretic repulsion, which in turn prevents the deposition of a second nanocrystal nearby. Thermodiffusion coefficients are normally positive meaning particles move from hotter regions to colder ones. In some cases, however, highly charged nanocrystals in solutions of high ionic strength diffuse towards hotter regions – this effect was used by Lin et al. to laser print clusters of plasmonic nanocrystals.[98] Others have used phase masks to tune the optical beam shape in order to deposit lines and arrays of nanocrystals.[99] Two lasers are employed to control the orientation of printed gold nanorods and then deposit them within 1 s,[100] while a spatial light modulator enables the printing of an 8 x 8 array of 80 nm Au nanocrystals in 10 s (figure 7b),[93] while in another case selective printing of differently shaped gold nanocrystals from mixtures in suspension was demonstrated.[101] While these experiments all represent significant advances in the optical printing of single nanocrystals from suspension, challenges remain. Specifically, these techniques have been widely applied only to plasmonic materials such as Au and Ag. More studies of its application to insulating or semiconducting materials are needed.[95e] Methods to facilitate parallel printing are also needed for this method to reach commercial application.

3.5 Directed Chemical Assembly with DNA

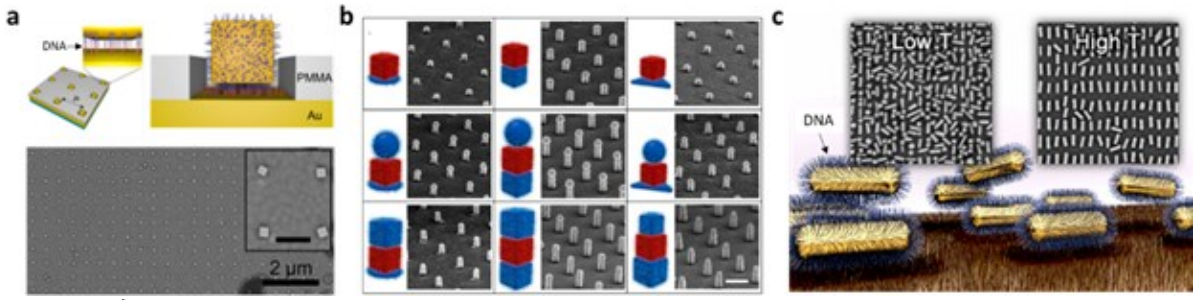

Figure 8: Summary of directed chemical assembly with DNA. (a) DNA assisted direct assembly. Single strand DNA was functionalized on the surface of gold nanocubes. The complementary DNA strand was selectively functionalized at the bottom of the template cavities. The bonding between two DNA strands drives the particles to assemble as designed. Adapted with permission.[102] Copyright 2015, American Chemical Society. (b) Scanning electron microscope and corresponding schematic illustration of 1D gold nanoparticle superstructures assembled by DNA. Adapted with permission.[103] Copyright 2018, American Association for the Advancement of Science (c) DNA-assisted temperature dependent direct assembly of oriented gold nanorod arrays. Adapted with permission.[104] Copyright 2019, American Chemical Society.

A number of different chemical functionalities have been used to achieve directed chemical assembly, such as diblock copolymers, amide coupling chemistries, and thiolated self-assembled monolayers,[105] but DNA offers exceptional versatility albeit at the higher cost of synthesis.

One of the most selective and versatile chemical binding motifs for directed assembly is between nucleic acids in the DNA molecule.[106] Over the past two decades, DNA nanotechnology has rapidly grown into one of the most powerful tools for constructing assemblies of nanocrystals for use in applications ranging from optical devices[107] to drug-delivery.[108] To assemble discrete structures in solution, there are two common approaches: Firstly, the nanocrystals of interest are functionalized with ssDNA that only binds to specific locations on either a DNA scaffold or ssDNA on another nanocrystal.[109] Secondly, the nanocrystals are functionalized with ssDNA that assembles with other ssDNA where the nanocrystals form a part of the lattice, i.e. they are the tiles in a lattice.[110] These structures in solution, or alternatively single ssDNA functionalized nanocrystals, can then be bound via specific DNA motifs, or electrostatically, to lithographically defined patterns on a substrate to realize highly accurate printing of higher-order nanocrystal assemblies.[107]

One method to facilitate the DNA-mediated and deterministic assembly of single nanocrystals in 2D arrays is to use lithographic templates to define binding nodes for DNA-coated nanocrystals.[111] The Mirkin group has recently described this method in a number of publications.[103, 112] Briefly, they used electron-beam lithography to write patterns in a thin PMMA film on a gold surface which was functionalized with rigid and thiolated DNA strands. Metallic nanocrystals in suspension were functionalized with the complementary DNA strand, which resulted in their hybridization and assembly into the cavities in the PMMA substrate. These pores were lithographically defined such that only one nanocrystal could assemble at each node. This resulted in high assembly yields (>98%) with minimal non-specific adsorption of gold nanocubes and nanospheres.[112a] As an example of an

application for this technique, they assembled nanocubes of two different sizes in two overlaid patterns and when viewed at the two different resonance wavelengths of the cubes, the two spectrally-encrypted patterns were extracted.[112b]

As a first approximation, the adsorption of nanocrystals to substrates can be modelled via the Langmuir adsorption isotherm, where the surface coverage is determined only by the concentration of nanocrystals as well as their adsorption and desorption rate constants.[113] When the substrate is composed of binding nodes within a polymer pore, it has been shown that the assembly kinetics still obey the Langmuir adsorption model.[112c] However, the kinetics drastically change, depending on the pore depth and rapidly slows down with increasing depth. Thus, rapid assembly necessitates a pore with thickness around the same dimension as the nanocrystal. However, one advantage of a deep pore and DNA-based assembly, is that nanocrystals of alternating complementary strands can be vertically stacked inside the pore with remarkable control.[103, 112c] Figure 8b shows this for the case of nanocubes and nanospheres of various dimensions, vertically stacked via DNA-based assembly into lithographic patterns.

The techniques described in this section, and the preceding sections 3.2 and 3.3, largely rely on the fabrication of a template with confined patterns, often via electron beam lithography. While this is neither scalable nor economical, advances in both nanoimprint lithography and block-copolymer lithography promise a potentially scalable and economical route towards nanofabrication of these templates. However, to date the studies describing DNA-based assembly of nanocrystal arrays on 2D substrates require long equilibration times, typically 12-24 hours, which means these methods will apply predominantly to high-value niche applications.

4. Electrophoretic Deposition and Single Nanocrystal Array Assembly

4.1 The Principles of Electrophoresis and Electrophoretic deposition

Electrophoretic deposition (EPD) is a method used to deposit charged materials onto an electrically conductive surface. It has been extensively studied since the 19th century[114].[115] The particles themselves must bear a net surface charge. This is commonly the case since surface charge is usually employed to stabilize the particles against aggregation in polar media (such as water). Zeta potential (ζ) is the most important particle parameter and in the simplest case is a function of the charge on the surface of particle, the particle radius, the salt concentration and temperature.[116] For a particle in aqueous solution, surface charges may arise on the surface due to redox reactions (e.g. on gold or silver nanocrystals), surface acid-base reactions (e.g. on silica or latex) or adsorption of ions, polyelectrolytes and surfactants from solution.[117] The zeta potential can be determined experimentally by measuring the particle mobility in a DC electric field and applying Smoluchowski's equation[118] [1]:

$$\mu = \frac{v}{E} = \frac{2}{3}\frac{\varepsilon_0 \varepsilon_r \xi}{\eta} f(\kappa r) \quad [1]$$

Here μ is the mobility the particle and defined as its velocity v, divided by the strength of the applied electric field, E, $\varepsilon_0$is the vacuum permittivity, $\varepsilon_r$is the relative permittivity of the solvent, η is the viscosity of the solvent and $f(\kappa r)$ is a function, which depends on the particle radius (r) and the electrical double layer thickness (κ^{-1}).[117b] In turn, the double layer thickness (κ^{-1}) is determined by [119]:

$$\kappa^{-1} = \left(\frac{\varepsilon_r \varepsilon_0 kT}{2cz_i^2 e_0^2}\right)^{\frac{1}{2}} \quad [2]$$

Here k is the Boltzmann constant, z is the ion charge, e_0 is the elementary charge and c is the concentration of 1:1 electrolyte. Importantly, equations [1] and [2] explain the key parameters that determine the velocity of a particle in an electric field. These parameters are (1) the electric field strength, E; (2) the salt concentration, c, which determines κ, and (3) the zeta potential, ζ, which controls the susceptibility of the particle to the applied field. The particle size also plays a complex role through $f(\kappa r)$.

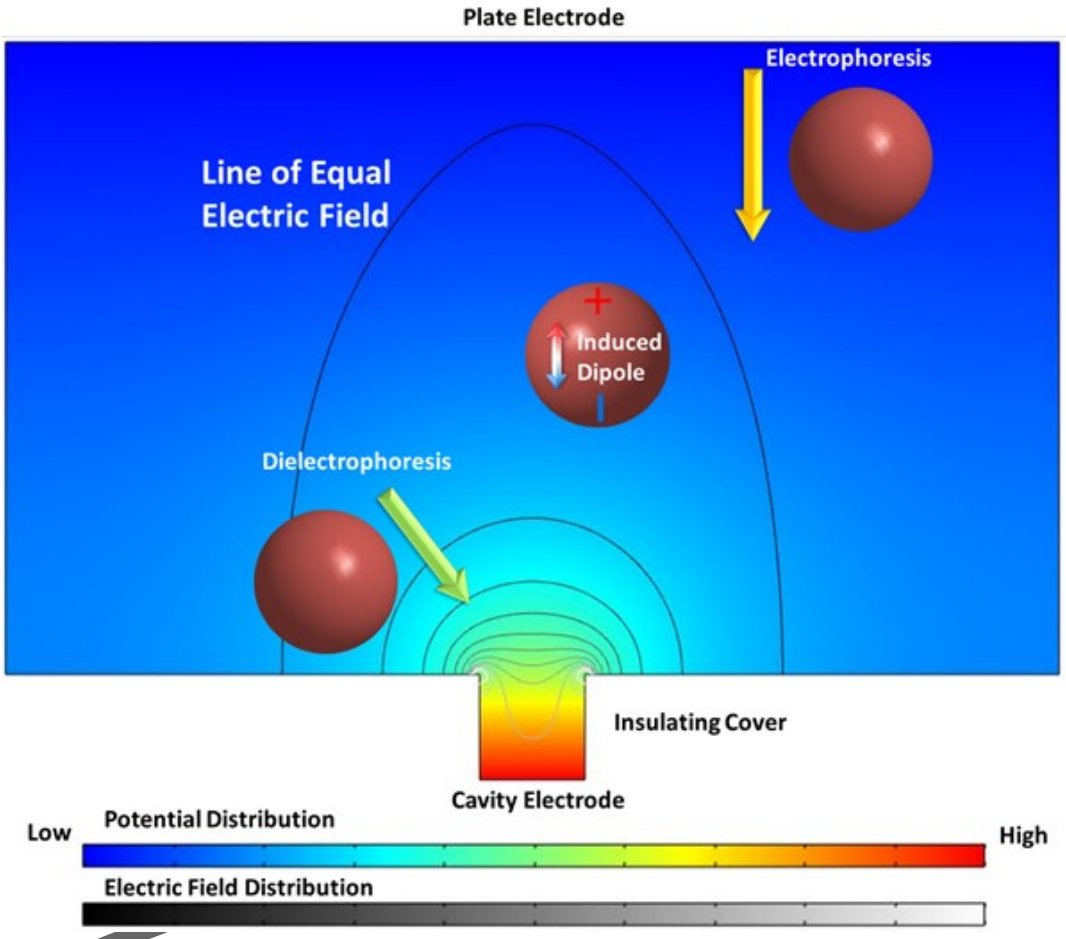

Figure 9: Schematic image to illustrate three aspects affecting the motion of nanoparticles during patterned-template, electrophoretic deposition. Electrophoresis is driven by the electric field generated externally between two electrodes. An induced dipole on a particle can control orientation and induce asymmetric nanoparticle assembly. Dielectrophoresis (DEP) is driven by the interaction of an induced or permanent dipole in a nanocrystal with an electric field gradient. DEP directs the particle towards regions of higher electric field strength.[116]

In reality, the applied electric field can influence nanocrystals in the solvent by two distinct, mechanisms: electrophoresis and dielectrophoresis. The first describes the direct Coulomb interaction between the charged nanocrystal and the electric field E, generated on the electrodes:

$$F_{EP} = Q_{eff}E \quad [3]$$

where Q_{eff} is the effective charge of the nanocrystals, approximated by:

$$Q_{eff} = 4\pi\zeta\varepsilon_r\varepsilon_0 r \quad [4]$$

where ζ is the zeta potential, ε_r is the relative dielectric constant of the solvent, ε_0 is the vacuum permittivity, and r is the radius of the nanocrystal.

The second force is dielectrophoresis, which originates from the non-uniform electrical field generated by the surface charge patterns. This field induces a dipole in the nanocrystals by distorting the surrounding electrical double layer. The interaction of this dipole with the non-uniform electrical field results in dielectrophoretic forces, given by:

$$F_{DEP} = p_{ef} \cdot \nabla E \quad [5]$$

where p_{ef} is the field induced dipole. For spherical nanocrystals the dielectrophoretic force can be expressed as:

$$F_{DEP} = 2\pi r^3 \varepsilon_r \varepsilon_0 Re[K]\nabla E^2 \quad [6]$$

where Re[K] is the real part of the Clausius–Mossotti factor K:

$$K = (\varepsilon_{NC}^* - \varepsilon_r)/(\varepsilon_{NC}^* + 2\varepsilon_r^*) \quad [7]$$

where ε_{NC}^* and ε_r^* are the complex permittivities of the nanocrystals and the solvent, respectively.

The above equations show that if the nanocrystals are more polarizable than the solvent they are dispersed in, they will always be attracted to regions of high electric field gradient, irrespective of the sign of their surface charge. Conversely, if the nanocrystals have a lower polarizability than the solvent then they will be repelled from regions of high electric field gradient. Thus, metallic and most semiconducting nanocrystals are attracted by dielectrophoretic forces to the edges of charge patterns where the changes in the electrical field strength are greatest.[120]

Generally, the electrophoretic force is longer ranged and stronger than the dielectrophoretic force for highly charged nanocrystals. However, weakly charged nanocrystals may experience stronger dielectrophoretic forces and be attracted to surface charges of either polarity. This was shown by Palleau, Sangeetha and Ressier for the case of 14 nm gold nanocrystals (figure 6b) in ethanol (strong electrophoretic forces) and 10 nm silver nanocrystals in hexane (stronger dielectrophoretic forces), where in both case the electrostatic

force was more than sufficient to overcome drag forces, van der Waals forces, and forces associated with Brownian motion.[76] Figure 9 shows the simulated electric field distribution between a cavity electrode at the bottom and a flat counter electrode at the top. It also illustrates the different behaviors of nanoparticles in such electric field systems. For distances relatively far from the cavity electrodes, the potential distribution is parallel to the plate electrodes.[121] Hence, particles experience an electric force normal to the target electrode and their migration can be determined from the electrophoretic mobility, given by Smoluchowski's equation [1]. Once the particle migrates closer, the electric field distribution starts to be distorted, due to the cavity geometry. The highest electric field is located at the cavity electrode and decreases with distance in a complex radial fashion. The decay length is determined by the double layer thickness (Equation [2]). Such electric field gradients lead to translational migration of the particle. At small separations from the cavity, DEP may become an important factor for precise positioning into the cavity. For non-spherical particles another important factor is the induced torque which may determine the orientation of the particle. The torque on an elongated prolate ellipsoidal particle can be described as follow[122]:

$$\vec{\boldsymbol{T}} = \vec{p} \times \vec{E} = \left(\alpha_0 \cdot \vec{E}\right) \times \vec{E} = -\Delta\alpha_0 \cos\theta \sin\theta \, E^2 \quad [8]$$

$$\alpha_{axis} = \varepsilon_0 V \left(\frac{\varepsilon_{particle} - \varepsilon_{medium}}{\varepsilon_{medium} + L_{axis}(\varepsilon_{particle} - \varepsilon_{medium})} \right) \quad [9]$$

$$L_{long} = \frac{1-e^2}{2e^3}\left[\ln\left(\frac{1+e}{1-e}\right) - 2e\right] \text{ and } L_{short} = \frac{1-L_{long}}{2} \quad [10]$$

Here, $\vec{\boldsymbol{T}}$ is the torque applied to the particle, $\vec{p}$ is the induced dipole moment, α_0 is the polarizability tensor of the particle, $\Delta\alpha_0 = \alpha_{long} - \alpha_{short}$ is the difference between the longitudinal and transverse polarizabilities, $\varepsilon_{particle}$ and ε_{medium} are the relative permittivities of the particle and medium respectively, V is the volume of the particle, L_{axis} is the depolarization factor along the long or short axis, and $e = \sqrt{1 - (b^2/a^2)}$ is the eccentricity of the particle ($a = length\ and\ b = width$).

This torque generated by the external electric field can be used to orient elongated nanoparticles during EPD. Apart from these three forces discussed above, there are other factors that also play a role in direct EPD assembly, such as electroosmosis and electrohydrodynamic flow which also affect the fluid motion around the particles and near the electrode interface, and both translational and rotational Brownian motion are critical contributors to the net particle motion during EPD assembly. However, these have not been quantified for single nanocrystal deposition to date.

4.2 Electrophoretic Deposition of Single Nanocrystal Arrays

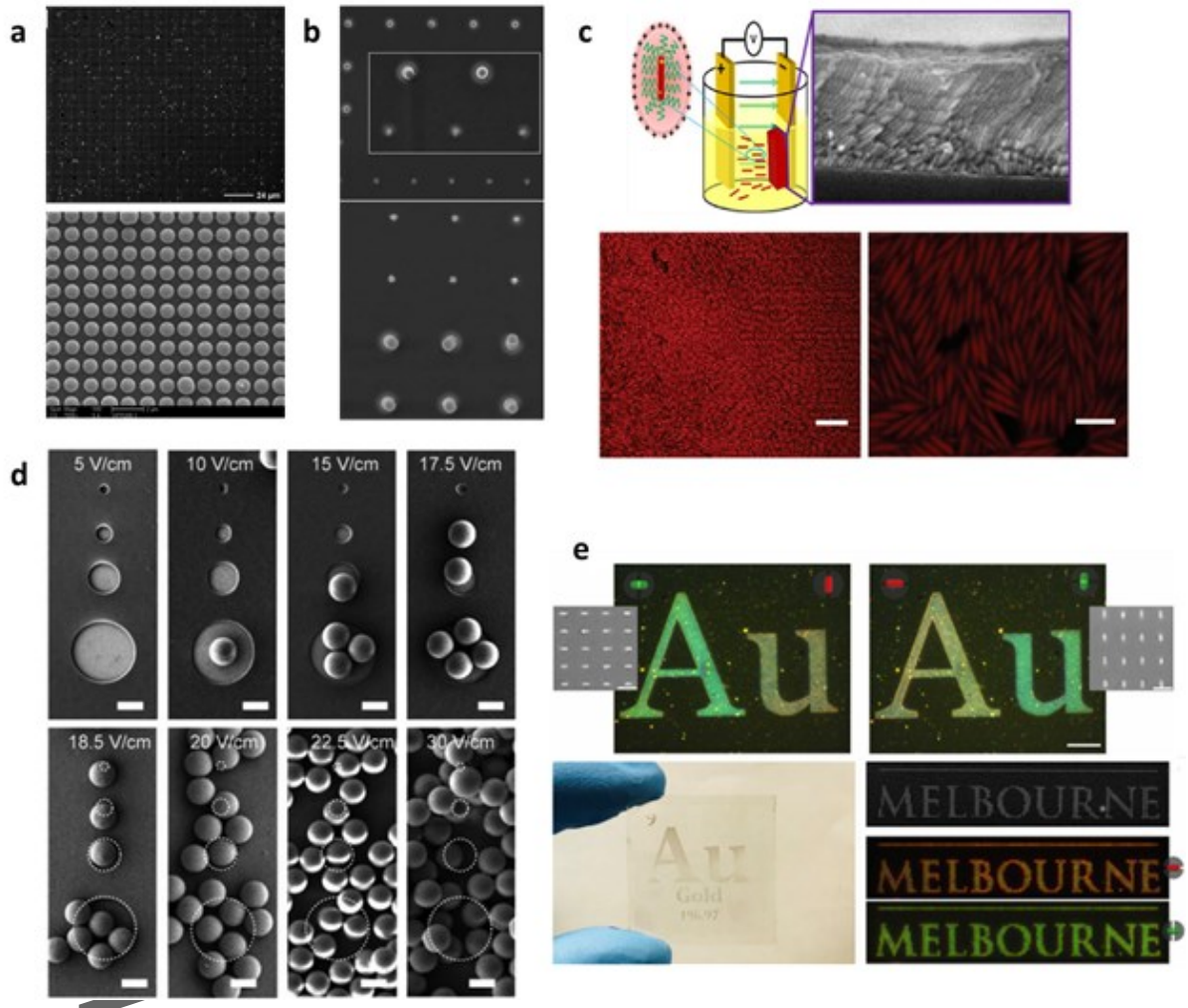

Figure 10: Summary of current development of single nanocrystal EPD. (a) Assembly of micron-sized polystyrene latex (PSL) particle arrays with nearly 100% assembly yield. Adapted with permission.[123] Copyright 2009, The Royal Society of Chemistry. (b) Template controlled size-selective assembly of different sizes of PSL nanoparticles. Adapted with permission.[124] Copyright 2011, American Chemical Society. (c) Electric field-controlled assembly with specific orientation of asymmetric nanoparticles. The induced dipole results in a vertical orientation. Reproduced with permission.[125] Copyright 2012, American Chemical Society. And optimization of the electrophoretic forces and rotational diffusion due to Brownian motion results in an oriented close packing on the surface of the electrode. Adapted with permission.[126] Copyright 2012, Wiley-VCH. (d) Electric field-controlled deposition process for PSL particles. Reproduced with permission.[127] Copyright 2015, American Chemical Society. (e) Large scale assembly of single gold nanorod arrays with almost 100% alignment. The polarization dependent color changes of the letters A and u is achieved due to the high degree of alignment. Adapted with permission.[128] Copyright 2018, American Chemical Society.

The start of direct EPD assembly for nanocrystals dates back to the early 1990s. Giersig et al. reported the formation of hexagonal close packed gold nanoparticle monolayers by EPD.[129] A graphite electrode and Al-foil counter electrode were used and an applied potential of 50 mV across a 2 mm spacing was used to deposit tri-sodium citrate stabilized colloidal gold nanoparticles. This work demonstrated that controlled deposition of nanoscale particle by EPD method was possible and that dense monolayers with well-defined particle spacings

could be achieved, Thereafter, there has been considerable investigation of the possibilities of EPD for both micron sized particles as well as nanoparticles.[130]

Initial work resulted in closely packed particle patterns on the substrates. In 2009, Barbee et. al. demonstrated direct EPD based assembly of latex (PSL) nanoparticles.[123] Single PSL particles can be precisely controlled and deposited into the photolithography patterned substrate. In their report, a template with sub-micrometer size cavities were patterned by photolithography and carefully assembled into a cell for EPD assembly. Hundreds of millions of PSL microbeads were precisely deposited into cavities with the help of a DC electric field in less than a minute. More than 99% of cavities were filled with single particles. Their experiments demonstrated the potential of direct EPD for single particle assembly. Following their work, in 2011, S. Siavoshi and A. Busnaina et. al. investigated the effect of the cavity size for directly EDP assembly.[124] Unlike earlier work, they used polystyrene particles with sizes of 200 nm and 50 nm as assembly targets. A dual-cavity template was fabricated by EBL with two sets of cavities with dimensions close to those of the PSL particles. Assembly was performed by applying a DC electric field. The larger particles were firstly deposited followed by the smaller particles. With careful control of the applied potential and the deposition time, the two different size particles could be sorted and deposited into different sized cavities, on the same template. They also reported that multiple small particles could be deposited into one large cavity.

Singh et al. have reported the assembly of vertically aligned 20 nm CdS nanorods by EPD.[125] They used the property that elongated particles experience a torque derived from the induced dipole in an external electric field and this orients the particles along the direction of the applied electric field. Up to 9 layers (~400 nm) of closely packed, vertical nanorod arrays were deposited over 3 minutes. Solomon has discussed the interplay of the parameters that determine the quality of EPD assembly of nanomaterials.[126, 131] They used ellipsoidal polystyrene particles in a study of EPD onto a plate electrode. Their results revealed that there is a critical electric field range in which the ellipsoids packed regularly onto the surface of electrode. Above or below this electric field range, the ellipsoids packed more randomly. They proposed that deposition is strongly determined by the colloid Peclet number. This accounts for the competing forces due to electrophoresis, which tends to align particles with the applied field and Brownian motion which tends to randomize the particles. The competition and balance between electric field generated movement and Brownian motion can lead to different positioning and can be controlled by the colloid properties and electric fields. A further controllability and quality study of direct EPD assembly for single particles was performed by F. Qian and T. Y. Olson in 2014.[127] They carefully studied the effects of the electric field and template size during EPD assembly. Following optimization, they were able to fabricate multi-particle unit arrays.

4.3 Perspective in Electrophoretic Deposition Assembly

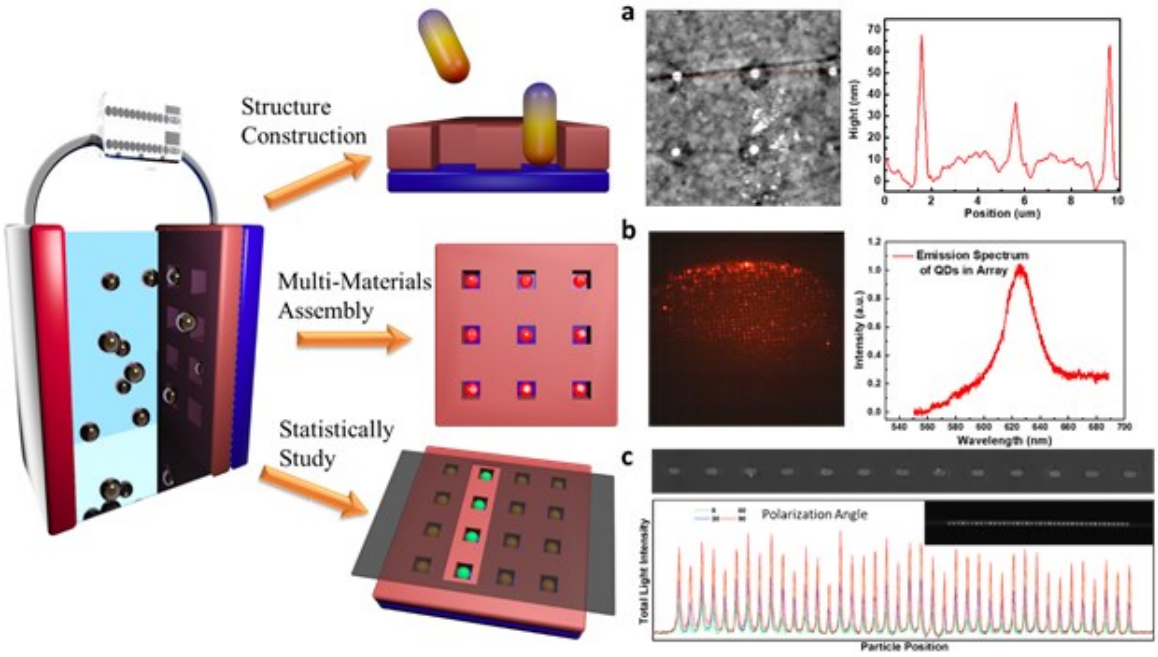

Figure 11: The potential of EPD assembly. (a) Nanorods may be deposited both vertically and horizontally. AFM characterization and height profile of an array of vertically oriented gold nanorods. (b) EPD of an array of quantum dots. (c) Statistical studies of large numbers of single nanocrystals is facilitated by array formation. SEM image and polarization-dependent gold nanorod scattering intensity from an array of gold nanorods. Adapted with permission.[57] Copyright 2018, American Chemical Society.

The investigation of EPD assembly has been underway for a decade. It has evolved from the preparation of close packed particle assemblies to the controlled assembly of single nanocrystal arrays with arbitrary shape and size and spacing and even orientation. Particularly exciting is that the external field induced dipole in a nanocrystal results in a torque that tends to align a nanocrystal with the applied electric field. The torque is also present on a charged rod. As a result, it is possible to deposit rods either vertically or horizontally (figure 10a). EPD also has the potential to be a universal assembly method. As long as the target particles carry a charge and are colloidally stable in solution, then in principle, with proper optimization, they can be assembled *via* EPD. Figure 10b shows a wide-field microscopy fluorescence image and fluorescence spectra of an array of semiconductor (CdSe/CdS/ZnS) quantum dots. The quantum dots were synthesized in an organic solvent and phase transferred into the aqueous phase with negatively charged polymers. This demonstrates that both conducting and insulating materials are amenable to EPD.

5. Conclusion

Fabrication of single nanocrystal array holds great potential as a platform to create addressable and functional materials. It offers nanometer spatial resolution, the ability to deposit a wide range of materials, multiplexing, and relatively easy scalability. In this review, five of the most promising, direct assembly methods have been discussed. Each of those methods has proved to be useful for a certain type of direct assembly.

CFA has the potential to be adapted to most kinds of nanocrystal assembly since the assembly is driven by the capillary force between liquid, air, solid interface. But CFA assembly is sensitive to the ambient humidity, surface roughness of the template, temperature of the assembly system and the presence of excess surfactant in the solution. Electrostatic assembly has the advantage that it requires a simple set-up and is amenable to large scale processing. However, deposition is limited by diffusion, and consequently, electrostatic assembly often requires a long time (2 - 24 h) for complete deposition. An additional disadvantage of electrostatic assembly is the complex surface chemistry and surface functionalization needed to direct nanocrystals into the cavities. Optical printing assembly methods do not require a prefabricated substrate as the assembly template. The laser driven assembly also provides a high degree of freedom in terms of array construction. However, spatial resolution of the printed arrays is only micron-scale at best. Directed chemical assembly with DNA cedes nanoscale precision in terms of nanocrystal positioning and also offers accurate assembly of three dimensional structures. However, as with electrostatic assembly, DNA assisted assembly is also a relatively slow process while the complexity and cost of surface DNA functionalization also limits its applications. Finally, we note that for EPD assembly, the assembly time is as short as a few seconds to minutes and it offers high accuracy over relatively large substrate areas. It also has the potential to be applied to most kinds of nanomaterials which can be stabilized in aqueous solution. However, EPD assembly requires a conducting template which does limit the choice of substrate. Furthermore, the high field strengths may damage particles on contact with the electrode during deposition. Therefore, it remains to be seen which methods can yield single nanocrystal arrays which are durable and robust enough for archiving and for commercial implementation. At the very least these methods offer an approach to more systematic studies of single nanocrystals, a field which is hampered by the difficulty of carrying out statistically meaningful measurements.

Acknowledgements

The authors thank the Australian Research Council for support under Grant CE170100026. We also acknowledge the support of the USAF through AOARD Grant FA2386-13-1-4072. C.K. acknowledges support from a ResearchPlus Postdoctoral Fellowship (CSIRO Manufacturing).

Conflict of Interest

The authors declare no conflict of interest.

Reference:

[1] P. Mulvaney, *Langmuir* **1996**, *12*, 788.

[2] S.-H. Han, H.-M. Liu, J. Bai, X. L. Tian, B. Y. Xia, J.-H. Zeng, J.-X. Jiang, Y. Chen, *ACS Appl. Energy Mater.* **2018**, *1*, 1252.

[3] K. Saito, T. Tatsuma, *ACS Photonics* **2016**, *3*, 1782.

[4] K. W. Song, R. Costi, V. Bulović, *Adv. Mater.* **2013**, *25*, 1420.

[5] Z. Ni, L. Ma, S. Du, Y. Xu, M. Yuan, H. Fang, Z. Wang, M. Xu, D. Li, J. Yang, *ACS Nano* **2017**, *11*, 9854.

[6] a) A. Biswas, I. S. Bayer, A. S. Biris, T. Wang, E. Dervishi, F. Faupel, *Adv. Colloid Interface Sci.* **2012**, *170*, 2; b) H. Jans, Q. Huo, *Chem. Soc. Rev.* **2012**, *41*, 2849; c) R. V. Martínez, J. Martínez, R. Garcia, *Nanotechnology* **2010**, *21*, 245301; d) S. Pan, D.-D. Zeng, H. Zhang, H. Li, *Appl. Phys. A* **2000**, *70*, 637.

[7] A. Kosiorek, W. Kandulski, H. Glaczynska, M. Giersig, *Small* **2005**, *1*, 439.

[8] E. M. Akinoglu, A. J. Morfa, M. Giersig, *Langmuir* **2014**, *30*, 12354.

[9] F. Song, H. Su, J. Han, J. Xu, D. Zhang, *Sens. Actuators, B* **2010**, *145*, 39.

[10] Y. Dong, B. Jia, F. Fu, H. Zhang, L. Zhang, J. Zhou, *Angew. Chem., Int. Ed.* **2016**, *55*, 13504.

[11] a) B. Ding, H. Wu, W. Xu, Z. Zhao, Y. Liu, H. Yu, H. Yan, *Nano Lett.* **2010**, *10*, 5065; b) A. C. Pearson, E. Pound, A. T. Woolley, M. R. Linford, J. N. Harb, R. C. Davis, *Nano Lett.* **2011**, *11*, 1981; c) A. M. Hung, C. M. Micheel, L. D. Bozano, L. W. Osterbur, G. M. Wallraff, J. N. Cha, *Nat. Nanotechnol.* **2010**, *5*, 121.

[12] C. Tabor, D. Van Haute, M. A. El-Sayed, *ACS Nano* **2009**, *3*, 3670.

[13] Y. Huang, W. Li, M. Qin, H. Zhou, X. Zhang, F. Li, Y. Song, *Small* **2017**, *13*.

[14] M. Mesch, B. Metzger, M. Hentschel, H. Giessen, *Nano Lett.* **2016**, *16*, 3155.

[15] a) Y. Chen, *Microelectron. Eng.* **2015**, *135*, 57; b) C. Vieu, F. Carcenac, A. Pepin, Y. Chen, M. Mejias, A. Lebib, L. Manin-Ferlazzo, L. Couraud, H. Launois, *Appl. Surf. Sci.* **2000**, *164*, 111; c) L. T. Varghese, L. Fan, Y. Xuan, C. Tansarawiput, S. Kim, M. Qi, *Small* **2013**, *9*, 3778; d) W. Chen, M. Tymchenko, P. Gopalan, X. Ye, Y. Wu, M. Zhang, C. B. Murray, A. Alu, C. R. Kagan, *Nano Lett.* **2015**, *15*, 5254.

[16] S. Zankovych, T. Hoffmann, J. Seekamp, J. U. Bruch, C. M. S. Torres, *Nanotechnology* **2001**, *12*, 91.

[17] H. Schift, A. Kristensen, *Nanoimprint Lithography – Patterning of Resists Using Molding*, in *Springer Handbook of Nanotechnology*, (Ed: B. Bhushan), Springer Berlin Heidelberg, Berlin, Heidelberg **2010**, 271.

[18] S. H. Ahn, L. J. Guo, *Adv. Mater.* **2008**, *20*, 2044.

[19] a) R. Garcia, A. W. Knoll, E. Riedo, *Nat. Nanotechnol.* **2014**, *9*, 577; b) Y. K. Ryu Cho, C. D. Rawlings, H. Wolf, M. Spieser, S. Bisig, S. Reidt, M. Sousa, S. R. Khanal, T. D. B. Jacobs, A. W. Knoll, *ACS Nano* **2017**, *11*, 11890.

[20] G.-Y. Liu, S. Xu, Y. Qian, *Acc. Chem. Res.* **2000**, *33*, 457.

[21] K. M. Carroll, X. Lu, S. Kim, Y. Gao, H.-J. Kim, S. Somnath, L. Polloni, R. Sordan, W. P. King, J. E. Curtis, E. Riedo, *Nanoscale* **2014**, *6*, 1299.

[22] a) Y. Dong, E. M. Akinoglu, H. Zhang, F. Maasoumi, J. Zhou, P. Mulvaney, *Adv. Funct. Mater.* **2019**, *0*, 1904290; b) G. Richter, K. Hillerich, D. S. Gianola, R. Mönig, O. Kraft, C. A. Volkert, *Nano Lett.* **2009**, *9*, 3048.

[23] M. E. T. Molares, V. Buschmann, D. Dobrev, R. Neumann, R. Scholz, I. U. Schuchert, J. Vetter, *Adv. Mater.* **2001**, *13*, 62.

[24] a) A. J. Yin, J. Li, W. Jian, A. J. Bennett, J. M. Xu, *Appl. Phys. Lett.* **2001**, *79*, 1039; b) E. J. Menke, M. A. Thompson, C. Xiang, L. C. Yang, R. M. Penner, *Nat. Mater.* **2006**, *5*, 914; c) J. Guiliani, J. Cadena, C. Monton, *Nanotechnology* **2018**, *29*, 075301; d) X. Xia, J. Tu, Y. Zhang, X. Wang, C. Gu, X.-b. Zhao, H. J. Fan, *ACS Nano* **2012**, *6*, 5531.

[25] S. M. George, *Chem. Rev.* **2009**, *110*, 111.

[26] a) J. W. Elam, M. Biswas, S. Darling, A. Yanguas-Gil, J. D. Emery, A. B. Martinson, P. F. Nealey, T. Segal-Peretz, Q. Peng, J. Winterstein, *ECS Trans.* **2015**, *69*, 147; b) Y.-C. Tseng, Q. Peng, L. E. Ocola, D. A. Czaplewski, J. W. Elam, S. B. Darling, *J. Mater. Chem.* **2011**, *21*, 11722.
[27] J. Olson, A. Manjavacas, T. Basu, D. Huang, A. E. Schlather, B. Zheng, N. J. Halas, P. Nordlander, S. Link, *ACS Nano* **2015**, *10*, 1108.
[28] T. D. James, P. Mulvaney, A. Roberts, *Nano Lett.* **2016**, *16*, 3817.
[29] J. Hu, D. Wang, D. Bhowmik, T. Liu, S. Deng, M. P. Knudson, X. Ao, T. W. Odom, *ACS Nano* **2019**, *13*, 4613.
[30] A. Yang, T. B. Hoang, M. Dridi, C. Deeb, M. H. Mikkelsen, G. C. Schatz, T. W. Odom, *Nat. Commun.* **2015**, *6*, 6939.
[31] S. T. Zimmermann, D. W. R. Balkenende, A. Lavrenova, C. Weder, J. Brugger, *ACS Appl. Mater. Interfaces* **2017**, *9*, 41454.
[32] Y. Shen, J. Zhou, T. Liu, Y. Tao, R. Jiang, M. Liu, G. Xiao, J. Zhu, Z.-K. Zhou, X. Wang, C. Jin, J. Wang, *Nat. Commun.* **2013**, *4*, 2381.
[33] M. Li, R. B. Bhiladvala, T. J. Morrow, J. A. Sioss, K.-K. Lew, J. M. Redwing, C. D. Keating, T. S. Mayer, *Nat. Nanotechnol.* **2008**, *3*, 88.
[34] a) L. Shao, X. Zhuo, J. Wang, *Adv. Mater.* **2018**, *30*, 1704338; b) I. Pastoriza-Santos, C. Kinnear, J. Pérez-Juste, P. Mulvaney, L. M. Liz-Marzán, *Nat. Rev. Mater.* **2018**, *3*, 375; c) A. Kristensen, J. K. Yang, S. I. Bozhevolnyi, S. Link, P. Nordlander, N. J. Halas, N. A. Mortensen, *Nat. Rev. Mater.* **2017**, *2*, 16088; d) M. Hentschel, M. Schäferling, X. Duan, H. Giessen, N. Liu, *Sci. Adv.* **2017**, *3*, e1602735.
[35] a) S. Zhang, C. I. Pelligra, X. Feng, C. O. Osuji, *Adv. Mater.* **2018**, *30*; b) M. Grzelczak, J. Vermant, E. M. Furst, L. M. Liz-Marzán, *ACS Nano* **2010**, *4*, 3591.
[36] H. Chen, Z. Sun, W. Ni, K. C. Woo, H. Q. Lin, L. Sun, C. Yan, J. Wang, *Small* **2009**, *5*, 2111.
[37] N. Liu, T. Liedl, *Chem. Rev.* **2018**.
[38] R. Verre, L. Shao, N. Odebo Länk, P. Karpinski, A. B. Yankovich, T. J. Antosiewicz, E. Olsson, M. Käll, *Adv. Mater.* **2017**, *29*, 1701352.
[39] J. Kaschke, L. Blume, L. Wu, M. Thiel, K. Bade, Z. Yang, M. Wegener, *Adv. Opt. Mater.* **2015**, *3*, 1411.
[40] M. W. Knight, L. Liu, Y. Wang, L. Brown, S. Mukherjee, N. S. King, H. O. Everitt, P. Nordlander, N. J. Halas, *Nano Lett.* **2012**, *12*, 6000.
[41] E. Albisetti, K. M. Carroll, X. Lu, J. E. Curtis, D. Petti, R. Bertacco, E. Riedo, *Nanotechnology* **2016**, *27*, 315302.
[42] T. Kawawaki, H. Zhang, H. Nishi, P. Mulvaney, T. Tatsuma, *J. Phys. Chem. Lett.* **2017**, *8*, 3637.
[43] C. Li, K. L. Shuford, M. Chen, E. J. Lee, S. O. Cho, *ACS Nano* **2008**, *2*, 1760.
[44] H.-Y. Ahn, H.-E. Lee, K. Jin, K. T. Nam, *J. Mater. Chem. C* **2013**, *1*, 6861.
[45] A. Espinosa, A. K. A. Silva, A. Sánchez-Iglesias, M. Grzelczak, C. Péchoux, K. Desboeufs, L. M. Liz-Marzán, C. Wilhelm, *Adv. Healthcare Mater.* **2016**, *5*, 1040.
[46] A. B. Serrano-Montes, J. Langer, M. Henriksen-Lacey, D. Jimenez de Aberasturi, D. M. Solís, J. M. Taboada, F. Obelleiro, K. Sentosun, S. Bals, A. Bekdemir, F. Stellacci, L. M. Liz-Marzán, *J. Phys. Chem. C* **2016**, *120*, 20860.
[47] D. Jimenez de Aberasturi, A. B. Serrano-Montes, J. Langer, M. Henriksen-Lacey, W. J. Parak, L. M. Liz-Marzán, *Chem. Mater.* **2016**, *28*, 6779.
[48] B. Pelaz, P. del Pino, P. Maffre, R. Hartmann, M. Gallego, S. Rivera-Fernandez, J. M. de la Fuente, G. U. Nienhaus, W. J. Parak, *ACS Nano* **2015**, *9*, 6996.
[49] A. M. Funston, C. Novo, T. J. Davis, P. Mulvaney, *Nano Lett.* **2009**, *9*, 1651.
[50] N. A. Hatab, C.-H. Hsueh, A. L. Gaddis, S. T. Retterer, J.-H. Li, G. Eres, Z. Zhang, B. Gu, *Nano Lett.* **2010**, *10*, 4952.
[51] K. Boldt, N. Kirkwood, G. A. Beane, P. Mulvaney, *Chem. Mater.* **2013**, *25*, 4731.
[52] M. Pang, A. J. Cairns, Y. Liu, Y. Belmabkhout, H. C. Zeng, M. Eddaoudi, *J. Am. Chem. Soc.* **2013**, *135*, 10234.

[53] Y.-J. Lee, N. B. Schade, L. Sun, J. A. Fan, D. R. Bae, M. M. Mariscal, G. Lee, F. Capasso, S. Sacanna, V. N. Manoharan, *ACS Nano* **2013**, *7*, 11064.
[54] M. Mayer, A. M. Steiner, F. Röder, P. Formanek, T. A. F. König, A. Fery, *Angew. Chem., Int. Ed.* **2017**, *56*, 15866.
[55] J. Liu, Y. Lu, *J. Am. Chem. Soc.* **2003**, *125*, 6642.
[56] S. Wang, C. M. McGuirk, A. d'Aquino, J. A. Mason, C. A. Mirkin, *Adv. Mater.* **2018**, *30*, 1800202.
[57] H. Zhang, S. Zhang, Y. Wang, J. Si, Y. Chen, L. Zhuang, S. Chen, *ACS Appl. Mater. Interfaces* **2018**, *10*, 28664.
[58] D. Sun, S. Ma, Y. Ke, D. J. Collins, H.-C. Zhou, *J. Am. Chem. Soc.* **2006**, *128*, 3896.
[59] J. An, N. L. Rosi, *J. Am. Chem. Soc.* **2010**, *132*, 5578.
[60] a) T. Pinedo Rivera, O. Lecarme, J. Hartmann, E. Rossitto, K. Berton, D. Peyrade, *J. Vac. Sci. Technol., B: Microelectron. Nanometer Struct.--Process., Meas., Phenom.* **2008**, *26*, 2513; b) T. P. Rivera, O. Lecarme, J. Hartmann, R. Inglebert, D. Peyrade, *Microelectron. Eng.* **2009**, *86*, 1089.
[61] C. Kuemin, L. Nowack, L. Bozano, N. D. Spencer, H. Wolf, *Adv. Funct. Mater.* **2012**, *22*, 702.
[62] X. Zhou, Y. Zhou, J. C. Ku, C. Zhang, C. A. Mirkin, *ACS Nano* **2014**, *8*, 1511.
[63] V. Flauraud, M. Mastrangeli, G. D. Bernasconi, J. Butet, D. T. Alexander, E. Shahrabi, O. J. Martin, J. Brugger, *Nat. Nanotechnol.* **2017**, *12*, 73.
[64] T. Mapperson, Ph.D. Thesis, the University of Melbourne, **2017**.
[65] W. Han, M. Byun, Z. Lin, *J. Mater. Chem.* **2011**, *21*, 16968.
[66] C. Kuemin, R. Stutz, N. D. Spencer, H. Wolf, *Langmuir* **2011**, *27*, 6305.
[67] a) J. Henzie, S. C. Andrews, X. Y. Ling, Z. Li, P. Yang, *Proc. Natl. Acad. Sci. U. S. A.* **2013**, *110*, 6640; b) N. J. Greybush, I. Liberal, L. Malassis, J. M. Kikkawa, N. Engheta, C. B. Murray, C. R. Kagan, *ACS Nano* **2017**, *11*, 2917.
[68] Y. Cui, M. T. Björk, J. A. Liddle, C. Sönnichsen, B. Boussert, A. P. Alivisatos, *Nano Lett.* **2004**, *4*, 1093.
[69] J. A. Fan, K. Bao, L. Sun, J. Bao, V. N. Manoharan, P. Nordlander, F. Capasso, *Nano Lett.* **2012**, *12*, 5318.
[70] A. Rey, G. Billardon, E. Lörtscher, K. Moth-Poulsen, N. Stuhr-Hansen, H. Wolf, T. Bjørnholm, A. Stemmer, H. Riel, *Nanoscale* **2013**, *5*, 8680.
[71] T. Kraus, L. Malaquin, H. Schmid, W. Riess, N. D. Spencer, H. Wolf, *Nat. Nanotechnol.* **2007**, *2*, 570.
[72] J. A. Liddle, Y. Cui, P. Alivisatos, *J. Vac. Sci. Technol., B: Microelectron. Nanometer Struct.--Process., Meas., Phenom.* **2004**, *22*, 3409.
[73] M. J. Gordon, D. Peyrade, *Appl. Phys. Lett.* **2006**, *89*, 053112.
[74] S. Mehraeen, M. Asbahi, W. Fuke, J. K. Yang, J. Cao, M. C. Tan, *Langmuir* **2015**, *31*, 8548.
[75] M. Asbahi, S. Mehraeen, F. Wang, N. Yakovlev, K. S. L. Chong, J. Cao, M. C. Tan, J. K. W. Yang, *Nano Lett.* **2015**, *15*, 6066.
[76] E. Palleau, N. M. Sangeetha, L. Ressier, *Nanotechnology* **2011**, *22*, 325603.
[77] C. Kinnear, J. Cadusch, H. Zhang, J. Lu, T. D. James, A. Roberts, P. Mulvaney, *Langmuir* **2018**, *34*, 7355.
[78] D. Morales, L. Teulon, E. Palleau, T. Alnasser, L. Ressier, *Langmuir* **2018**, *34*, 1557.
[79] C. F. Carlson, U.S. Patent 2,297,691, **1942**.
[80] J. E. Stern, B. D. Terris, H. J. Mamin, D. Rugar, *Appl. Phys. Lett.* **1988**, *53*, 2717.
[81] H. O. Jacobs, A. Stemmer, *Surf. Interface Anal.* **1999**, *27*, 361.
[82] P. Mesquida, A. Stemmer, *Adv. Mater.* **2001**, *13*, 1395.
[83] a) H. O. Jacobs, G. M. Whitesides, *Sci.* **2001**, *291*, 1763; b) H. O. Jacobs, S. A. Campbell, M. G. Steward, *Adv. Mater.* **2002**, *14*, 1553; c) L. Teulon, Y. Hallez, S. Raffy, F. Guerin, E. Palleau, L. Ressier, *J. Phys. Chem. C* **2019**, *123*, 783; d) L. Ressier, E. Palleau, S. Behar, *Nanotechnology* **2012**, *23*, 255302; e) R. Diaz, E. Palleau, D. Poirot, N. M. Sangeetha, L. Ressier, *Nanotechnology* **2014**, *25*, 345302.

[84] M. Kolíbal, M. Konečný, F. Ligmajer, D. Škoda, T. Vystavěl, J. Zlámal, P. Varga, T. Šikola, *ACS Nano* **2012**, *6*, 10098.
[85] R. V. Martínez, J. Martínez, M. Chiesa, R. Garcia, E. Coronado, E. Pinilla-Cienfuegos, S. Tatay, *Adv. Mater.* **2010**, *22*, 588.
[86] L. L. Yang, B. Yan, W. R. Premasiri, L. D. Ziegler, L. Dal Negro, B. M. Reinhard, *Adv. Funct. Mater.* **2010**, *20*, 2619.
[87] a) H. Kim, J. Kim, H. Yang, J. Suh, T. Kim, B. Han, S. Kim, D. S. Kim, P. V. Pikhitsa, M. Choi, *Nat. Nanotechnol.* **2006**, *1*, 117; b) F. Otten, U. Auer, F. E. Kruis, W. Prost, F. J. Tegude, H. Fissan, *Mater. Sci. Technol.* **2002**, *18*, 717.
[88] D. Nepal, M. S. Onses, K. Park, M. Jespersen, C. J. Thode, P. F. Nealey, R. A. Vaia, *ACS Nano* **2012**, *6*, 5693.
[89] P. Moutet, L.-M. Lacroix, A. Robert, M. Impéror-Clerc, G. Viau, L. Ressier, *Langmuir* **2015**, *31*, 4106.
[90] H. Fudouzi, M. Kobayashi, N. Shinya, *Adv. Mater.* **2002**, *14*, 1649.
[91] a) C. R. Barry, M. G. Steward, N. Z. Lwin, H. O. Jacobs, *Nanotechnology* **2003**, *14*, 1057; b) D. Zhao, L. Duan, M. Xue, W. Ni, T. Cao, *Angew. Chem., Int. Ed.* **2009**, *48*, 6699; c) X. Ma, D. Zhao, M. Xue, H. Wang, T. Cao, *Angew. Chem., Int. Ed.* **2010**, *49*, 5537; d) J. J. Cole, C. R. Barry, X. Wang, H. O. Jacobs, *ACS Nano* **2010**, *4*, 7492.
[92] a) J. Gargiulo, I. L. Violi, S. Cerrota, L. Chvátal, E. Cortés, E. M. Perassi, F. Diaz, P. Zemánek, F. D. Stefani, *ACS Nano* **2017**, *11*, 9678; b) A. S. Urban, A. A. Lutich, F. D. Stefani, J. Feldmann, *Nano Lett.* **2010**, *10*, 4794.
[93] S. Nedev, A. S. Urban, A. A. Lutich, J. Feldmann, *Nano Lett.* **2011**, *11*, 5066.
[94] K. Svoboda, S. M. Block, *Opt. Lett.* **1994**, *19*, 930.
[95] a) A. Lehmuskero, P. Johansson, H. Rubinsztein-Dunlop, L. Tong, M. Käll, *ACS Nano* **2015**, *9*, 3453; b) O. M. Maragò, P. H. Jones, P. G. Gucciardi, G. Volpe, A. C. Ferrari, *Nat. Nanotechnol.* **2013**, *8*, 807; c) P. M. Bendix, L. Jauffred, K. Norregaard, L. B. Oddershede, *IEEE J. Sel. Top. Quantum Electron.* **2014**, *20*, 15; d) A. S. Urban, S. Carretero-Palacios, A. A. Lutich, T. Lohmüller, J. Feldmann, F. Jäckel, *Nanoscale* **2014**, *6*, 4458; e) M. L. Juan, M. Righini, R. Quidant, *Nat. Photonics* **2011**, *5*, 349.
[96] A. S. Urban, A. A. Lutich, F. D. Stefani, J. Feldmann, *Nano Lett.* **2010**, *10*, 4794.
[97] J. Gargiulo, S. Cerrota, E. Cortes, I. L. Violi, F. D. Stefani, *Nano Lett.* **2016**, *16*, 1224.
[98] L. Lin, X. Peng, M. Wang, L. Scarabelli, Z. Mao, L. M. Liz-Marzán, M. F. Becker, Y. Zheng, *ACS Nano* **2016**, *10*, 9659.
[99] Y. Bao, Z. Yan, N. F. Scherer, *J. Phys. Chem. C* **2014**, *118*, 19315.
[100] J. Do, M. Fedoruk, F. Jäckel, J. Feldmann, *Nano Lett.* **2013**, *13*, 4164.
[101] M. A. Huergo, C. M. Maier, M. F. Castez, C. Vericat, S. Nedev, R. C. Salvarezza, A. S. Urban, J. Feldmann, *ACS Nano* **2016**, *10*, 3614.
[102] Q. Y. Lin, Z. Li, K. A. Brown, M. N. O'Brien, M. B. Ross, Y. Zhou, S. Butun, P. C. Chen, G. C. Schatz, V. P. Dravid, K. Aydin, C. A. Mirkin, *Nano Lett.* **2015**, *15*, 4699.
[103] Q.-Y. Lin, J. A. Mason, Z. Li, W. Zhou, M. N. O'Brien, K. A. Brown, M. R. Jones, S. Butun, B. Lee, V. P. Dravid, K. Aydin, C. A. Mirkin, *Sci.* **2018**, *359*, 669.
[104] B. D. Myers, E. Palacios, D. I. Myers, S. Butun, K. Aydin, V. P. Dravid, *Nano Lett.* **2019**, *19*, 4535.
[105] X. Zhou, F. Boey, F. Huo, L. Huang, H. Zhang, *Small* **2011**, *7*, 2273.
[106] M. Bathe, P. W. K. Rothemund, *MRS Bull.* **2017**, *42*, 882.
[107] A. Gopinath, E. Miyazono, A. Faraon, P. W. K. Rothemund, *Nature* **2016**, *535*, 401.
[108] a) S. Surana, A. R. Shenoy, Y. Krishnan, *Nat. Nanotechnol.* **2015**, *10*, 741; b) J. Li, C. Fan, H. Pei, J. Shi, Q. Huang, *Adv. Mater.* **2013**, *25*, 4386; c) S. M. Douglas, I. Bachelet, G. M. Church, *Sci.* **2012**, *335*, 831.
[109] a) S. J. Barrow, A. M. Funston, X. Wei, P. Mulvaney, *Nano Today* **2013**, *8*, 138; b) A. Samanta, S. Banerjee, Y. Liu, *Nanoscale* **2015**, *7*, 2210.

[110] R. Chhabra, J. Sharma, Y. Ke, Y. Liu, S. Rinker, S. Lindsay, H. Yan, *J. Am. Chem. Soc.* **2007**, *129*, 10304.
[111] C. H. Lalander, Y. Zheng, S. Dhuey, S. Cabrini, U. Bach, *ACS Nano* **2010**, *4*, 6153.
[112] a) Q.-Y. Lin, Z. Li, K. A. Brown, M. N. O'Brien, M. B. Ross, Y. Zhou, S. Butun, P.-C. Chen, G. C. Schatz, V. P. Dravid, K. Aydin, C. A. Mirkin, *Nano Lett.* **2015**, *15*, 4699; b) Q.-Y. Lin, E. Palacios, W. Zhou, Z. Li, J. A. Mason, Z. Liu, H. Lin, P.-C. Chen, V. P. Dravid, K. Aydin, C. A. Mirkin, *Nano Lett.* **2018**, *18*, 2645; c) W. Zhou, Q.-Y. Lin, J. A. Mason, V. P. Dravid, C. A. Mirkin, *Small* **2018**, *14*, 1802742.
[113] M. N. O'Brien, B. Radha, K. A. Brown, M. R. Jones, C. A. Mirkin, *Angew. Chem., Int. Ed.* **2014**, *53*, 9532.
[114] W. F. Pickard, *J. Electrochem. Soc.* **1968**, *115*, 105C.
[115] P. Sarkar, P. S. Nicholson, *J. Am. Ceram. Soc.* **1996**, *79*, 1987.
[116] J. H. Dickerson, A. R. Boccaccini, *Electrophoretic deposition of nanomaterials*, Springer, **2011**.
[117] a) D. J. Shaw, B. Costello, *Introduction to colloid and surface chemistry: Butterworth-Heinemann, Oxford, 1991, ISBN 0 7506 1182 0, 306 pp,£ 14.95*, Elsevier, **1993**; b) L. Besra, M. Liu, *Prog. Mater. Sci.* **2007**, *52*, 1.
[118] M. von Smoluchowski, *Zeit. Phys. Chem* **1917**, *92*, 129.
[119] H. Hamaker, *Trans. Faraday Soc.* **1940**, *35*, 279.
[120] S. Lemonier, P. Moutet, W. Moussa, M. Destarac, L. Ressier, J.-D. Marty, *Gold Bull.* **2013**, *46*, 267.
[121] O. D. Velev, K. H. Bhatt, *Soft Matter* **2006**, *2*, 738.
[122] a) P. Zijlstra, M. van Stee, N. Verhart, Z. Gu, M. Orrit, *Phys. Chem. Chem. Phys.* **2012**, *14*, 4584; b) W. Ahmed, E. S. Kooij, A. van Silfhout, B. Poelsema, *Nano Lett.* **2009**, *9*, 3786.
[123] K. D. Barbee, A. P. Hsiao, M. J. Heller, X. Huang, *Lab on a Chip* **2009**, *9*, 3268.
[124] S. Siavoshi, C. Yilmaz, S. Somu, T. Musacchio, J. R. Upponi, V. P. Torchilin, A. Busnaina, *Langmuir* **2011**, *27*, 7301.
[125] A. Singh, N. J. English, K. M. Ryan, *J. Phys. Chem. B* **2012**, *117*, 1608.
[126] A. A. Advances in colloid and interface scienceShah, H. Kang, K. L. Kohlstedt, K. H. Ahn, S. C. Glotzer, C. W. Monroe, M. J. Solomon, *Small* **2012**, *8*, 1551.
[127] F. Qian, A. J. Pascall, M. Bora, T. Y.-J. Han, S. Guo, S. S. Ly, M. A. Worsley, J. D. Kuntz, T. Y. Olson, *Langmuir* **2015**, *31*, 3563.
[128] H. Zhang, J. Cadusch, C. Kinnear, T. James, A. Roberts, P. Mulvaney, *ACS Nano* **2018**, *12*, 7529.
[129] a) M. Giersig, P. Mulvaney, *Langmuir* **1993**, *9*, 3408; b) M. Giersig, P. Mulvaney, *J. Phys. Chem.* **1993**, *97*, 6334.
[130] X. Xiong, P. Makaram, A. Busnaina, K. Bakhtari, S. Somu, N. McGruer, J. Park, *Appl. Phys. Lett.* **2006**, *89*, 193108.
[131] A. A. Shah, M. Ganesan, J. Jocz, M. J. Solomon, *ACS Nano* **2014**, *8*, 8095.

Heyou Zhang is a Ph.D. student in the ARC Centre of Excellence in Exciton Science, School of Chemistry at the University of Melbourne, Australia. He received his B.Sc. (2013) in Chemistry from Wuhan University, China, and M.Sc. (2016) in Chemistry from the University of Melbourne, Australia. His research interests are focused on nanoscience, nanocrystal synthesis and assembly, single crystal spectroscopy and nanofabrication.

Calum Kinnear completed a Master's degree in Chemical Physics (The University of Edinburgh), a PhD in Chemistry (Adolphe Merkle Institute) with Prof. Alke Petri-Fink and Prof. Barbara Rothen-Rutishauser, and a Postdoctoral Fellowship in Chemistry (University of Melbourne) with Prof. Paul Mulvaney. He is currently a CERC Postdoctoral Fellow at CSIRO in Melbourne, Australia, researching nanocrystal assembly and integration into photocatalytic devices.

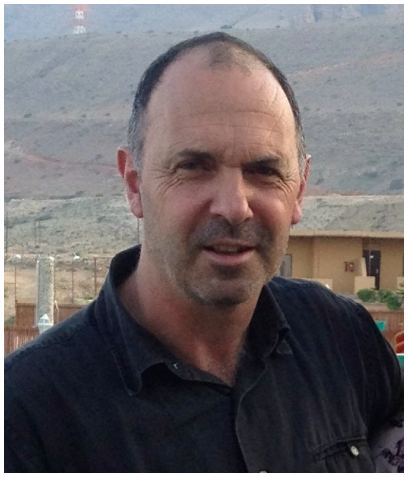

Paul Mulvaney is the Director of the ARC Centre of Excellence in Exciton Science and Professor of Chemistry in the School of Chemistry and Bio21 Institute at the University of Melbourne. His primary research field is nanocrystal spectroscopy.

TOC entry:

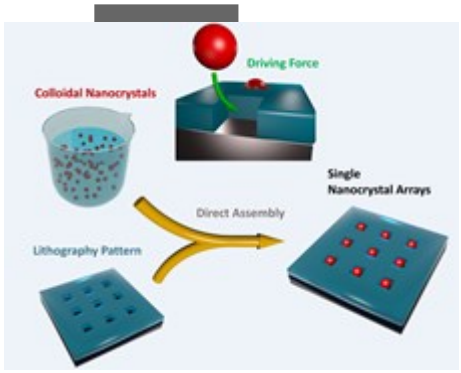

This review provides an overview of the direct assembly methods used to fabricate single nanocrystal arrays. Five principal methods used as well as the advantages and disadvantages of each are discussed. Potential future developments in the field are also presented.